48TH TURBOMACHINERY & 35TH PUMP SYMPOSIA
HOUSTON, TEXAS | SEPTEMBER 9-12, 2019
GEORGE R. BROWN CONVENTION CENTER

STABILITY CONSIDERATIONS OF CENTRIFUGAL COMPRESSORS EQUIPPED WITH ACTIVE MAGNETIC BEARINGS

Yves Bidaut
Manager Mechanical Development
MAN Energy Solutions Schweiz AG
Zurich, Switzerland

Reto Somaini
Mechanical Development
MAN Energy Solutions Schweiz AG
Zurich, Switzerland

Mônica Alves de Lima Ruguê
Mechanical Development
MAN Energy Solutions Schweiz AG
Zurich, Switzerland

Yves Bidaut is Manager of the mechanical development department of MAN Energy Solutions Schweiz AG in Zurich, Switzerland. His job function includes the development and analysis of the components of centrifugal compressors for the Oil & Gas application. He is responsible for providing technical support in rotordynamics and stress analysis. Before joining the site in Switzerland in 2003 he was employed for 6 years in MAN Energy Solutions, Berlin where he was involved in the design, finite element analysis, rotordynamic analysis, testing and development of centrifugal compressors. He received his diploma (Mechanical Engineering, 1995) from the University of Valenciennes (France).

Reto Somaini graduated as Mechanical Engineering in 2006 at the ETH (Swiss Federal Institute of Technology) in Zurich. Since then he's active for MAN Energy Solutions Schweiz AG, with a major focus on the care of magnetic bearing machines. The job tasks include rotordynamic support and analysis for the commissioned projects and technical bid support for the high speed compressors.

Mônica Ruguê joined MAN Energy Solutions Schweiz AG in 2018. She is mainly responsible for performing rotordynamic analysis for high speed compressors as well as static and dynamic finite element analysis for centrifugal compressors. She graduated as Mechanical Engineer in 2003 at the Darmstadt University of Technology. Before joining MAN she worked for 13 years in the pump industry with the main focus on rotordynamics of multiphase pumps for Subsea Applications.

ABSTRACT

Many centrifugal compressor rotordynamic stability investigations have been performed over the last 40 years. Rules, based on the large experience and knowledge gained from comprehensive experimental studies and numerical analyses performed by different institutes and OEMs, are defined to ensure compressor stability in operation. The API 617 standard combines the rules to define a standardized procedure that shall be valid for all compressors, manufacturer type or size independent. In the latest version of the API 617 standard (8th edition) the analysis is detailed more precisely to enhance stability prediction.

Up to the 7th edition these rules did not account for compressors equipped with bearings than other conventional oil-film bearings. The 8th edition added a separate normative procedure for AMB (Active Magnetic Bearing) equipped compressors in Annex E.

Centrifugal compressors with AMB are currently used for various applications (gas storage, pipe-line), but in the last decade they have been implemented in new areas such as upstream processes and even subsea. Therefore, AMB compressor technical challenges (e.g. increased operating pressures) are increasing because the AMB load capacity is lower than a comparable oil-film bearing and causes the rotordynamic stability to become a crucial issue.

This paper describes a standardized calculation procedure (based on the API rule) for reliable compressor stability determination. The procedure considers the paramount factors that influence the stability such as the annular seal coefficients, the AMB transfer functions, or the compressed fluid characteristics (fouling conditions). In particular, a comparison between conventional and AMB equipped compressors is drawn and the main differences are highlighted. This paper demonstrates that the standard API 617 procedure to assess stability based on cross-coupled stiffness is appropriate for conventional oil bearing machines. However this procedure is not sufficient to determine the stability threshold of AMB compressors. An AMB machine stability analysis shall also include radial force variation in order to provide suitable confidence that a demanding machine application will have safe and stable field operation.

INTRODUCTION

Current oil and gas application centrifugal compressor lateral vibration assessments are lateral response and stability analyses. The main lateral response analysis goal is the prediction of the critical speeds, the associated damping (Amplification Factors) and potential unbalance response amplitude issues (e.g. excessive magnitudes, insufficient separation margins, etc.). Another lateral response aim is to understand unbalance sensitivity that can be used to help determine balance correction masses and location required to ensure smooth rotor vibration operation on site. The main stability analysis goal is eigenmodes (natural frequencies with associated damping and modal deflection shapes) determination. Optimized rotor design that avoids potential rotordynamic instabilities then results from a combination of the above analytical investigations and empirical knowledge.

Increased compressor operational requirements in the 1970s caused vibration issues and the need for accurate rotordynamic stability assessment. This need initiated extensive and comprehensive studies to understand the rotor instability phenomenon and find a solution. Various investigation results (measurements or analytical studies) published over the last 30 years reveal the rotordynamic stability measurement and analysis evolution. Cloud et al. (2018) presented the famous Ekofisk case as basis to show how analytical tools have evolved and how they determine a corresponding modern rotor design. Kocur and Cloud (2013) report how test field compressor rotordynamic stability measurement can validate stability calculations and provide stable field operation demonstration.

However, this knowledge mainly concerns machines equipped with conventional fluid-film (oil) bearings. Although the labyrinth seal forces, that are important to judge the overall stability behaviour, are common for all bearing types (oil bearing and AMB), empirical equations established until now are based in most cases on units with oil bearings and form the basis for definitive compressor stability evaluation.

To date, the AMB equipped compressor rotordynamic analysis focusses on the lateral (and torsional) critical speeds determination and associated unbalance response analysis. Until 2014, the API standard defined no particular requirement for AMB equipped compressor stability assessment because the examination is made during controller layout stage (generally carried out by the AMB supplier). Hence, this topic did not necessarily belong to the OEM focus during the compressor design. Only since the 8th Edition some particular requirements are specified in the Annex E: for instance, a minimum damping shall now be achieved depending on the frequency and full stability analysis calculation criteria are now defined.

Several hundred AMB equipped compressors are now in operation around the world for different applications, mainly midstream gas storage or pipeline. Kleynhans et al. (2005) detail the main properties and the challenges related to compressor design for these applications and in particular the requirements on the (static) bearing loads, the separation margin between the first bending mode (based on a low bearing stiffness) and the maximum operating speed. More recently, Somaini et al (2012) addressed important safety relevant rotordynamic criteria and compared the lowest bending mode logarithmic decrement (damping) stability behaviour between different compressor configurations. Based on API 617 7th edition Level I criteria this analysis showed that the AMB compressor sometimes outclassed the oil bearing configurations (showing higher log dec and Q_0 values).

When comparing oil bearing with the AMB compressor applications it is apparent that most AMB compressors operate under dry and clean gas conditions (gas storage) or at rather low and medium pressure levels (below 200 bar). However, AMB centrifugal compressors are now implemented in new applications such as upstream processes. Dettwyler et al. (2016) published challenges an OEM encountered during the technology maturation for a subsea application. Hence, the demand for these compressors is increasing along with the technical challenges because the handled gas pressure increases and the possibility of liquid content in the gas can cause compressor fouling during operation. Figure 1 shows that AMB equipped compressors generally operate with low gas density in comparison to conventional compressors. Since the applications are progressing towards higher power density solutions, the rotordynamic characteristics of the rotor are affected, and therefore, even if the design of the compressor is such that it is still below the Fulton threshold limit (Figure 1), a detailed and reliable stability analysis is crucial.

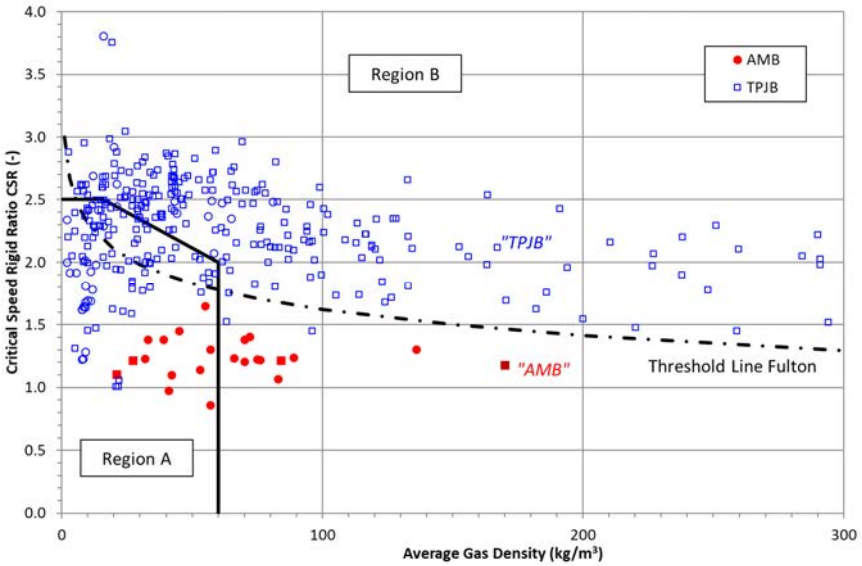

Figure 1: API 617 Level I Diagram with Fulton Line Showing Centrifugal Compressor References

AMB COMPRESSOR PARTICULARS

Bearings are the central compressor element to provide rotor system damping. There are specific load capacity and circumferential speed differences between oil-film and AMB, but the most significant difference is that AMB rotordynamic reaction to a shaft displacement and velocity is frequency dependent (ω). Oil bearings exhibit strong dependencies on shaft speed (Ω), specific load and the oil properties (Sommerfeld's Number). A magnetic bearing's response to a shaft displacement is isotropic, whereas isotropy is not necessarily attributed to TPJB. A five tilting pad bearing, for example, reacts with a force dependent of the shaft location relative to bearing bore in both horizontal and vertical direction. A position perturbation about the journal static equilibrium position can produce the calculated non-symmetrical stiffness and damping matrices that change as a function of Sommerfeld's number. In addition to the simple frequency dependent model, particularly tilting pad journal bearings (oil lubricated) can also produce frequency dependent (non-synchronous) coefficients models.

An AMB stator consists of a solenoid array with current fed coils and produces a pull effect force. The coil arrangement and current distribution provide arbitrary (radial) force direction. Normalizing the force magnitude by the resulting displacement yields the force gain and the resulting angle is the force phase. Figure 2 (left) illustrates the relationship between the forces and the AMB.

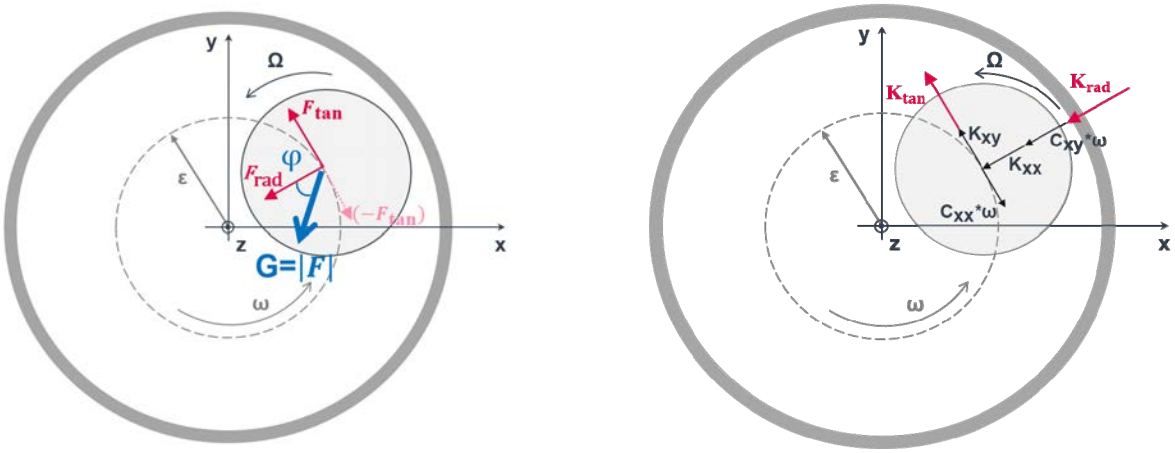

Figure 2: AMB resultant force on shaft (left), Seal impedance decomposition (right)

The reference coordinate system is the AMB stator with x and y directions and hence, the AMB force phase is different than the common phase lag in vibration monitoring devices that is based on a fixed base and observed rotor unbalance phase lag.

Equation 1 provides a generalized force reaction to rotor movement model:

$$\vec{F} = \begin{bmatrix} K_{xx} & K_{xy} \\ K_{yx} & K_{yy} \end{bmatrix} \begin{bmatrix} x \\ y \end{bmatrix} + \begin{bmatrix} D_{xx} & D_{xy} \\ D_{yx} & D_{yy} \end{bmatrix} \begin{bmatrix} \dot{x} \\ \dot{y} \end{bmatrix} \quad (1)$$

Isotropic bearings and annular seals apply the same rotor circular orbit with whirl frequency of ω and amplitude A model where the force is not dependent on eccentricity and angular position. Table 1 lists the associated mathematical expressions.

Table 1: Assumption for annular seals

For symmetric reaction to displacement:	For circular shaft orbit:
$K_{xx} = K_{yy},\ K_{xy} = -K_{yx}$ $D_{xx} = D_{yy},\ D_{xy} = -D_{yx}$	$\begin{bmatrix} x \\ y \end{bmatrix} = \begin{bmatrix} A\cos(\omega t) \\ A\sin(\omega t) \end{bmatrix}, \begin{bmatrix} \dot{x} \\ \dot{y} \end{bmatrix} = \begin{bmatrix} -A\omega\sin(\omega t) \\ A\omega\cos(\omega t) \end{bmatrix}, \begin{bmatrix} \ddot{x} \\ \ddot{y} \end{bmatrix} = \begin{bmatrix} -A\omega^2\cos(\omega t) \\ -A\omega^2\sin(\omega t) \end{bmatrix}$

Equation 2 below applies the above simplifications to resolve the radial and tangential forces in Figure 2 right side:

$$\begin{bmatrix} F_{rad} \\ F_{tan} \end{bmatrix} = A \begin{bmatrix} K_{xx} + C_{xy}\omega \\ K_{xy} - C_{xx}\omega \end{bmatrix} \quad (2)$$

Equation 3 below provides the corresponding gain (G) and the phase (φ):

$$G = \sqrt{F_{rad}^2 + F_{tan}^2} \qquad \varphi = \tan^{-1}\left(\frac{-F_{tan}}{F_{rad}}\right) \quad (3)$$

The advantage of the Gain/phase representation, rather than in coefficients, is clear assignment of force magnitude and direction. The magnitude can vary from increasing pressure fields, while the direction can remain constant for a given speed, geometry and inlet conditions. The phase directly indicates the induced force direction with respect to the rotor position.

The left plot in Figure 3 shows oil bearing (TPJB) characteristics expressed in stiffness and damping coefficients over the shaft rotational speed and the right plot shows the gain and phase characteristics comparison with a competing AMB. Because of the symmetric 4-tilting pad construction and load between pads, K_{xx} and K_{yy} are the same and the off-diagonal terms are virtually zero. The same is valid for the damping coefficients. Therefore, a single stiffness and damping curve is sufficient to describe the bearing force characteristics.

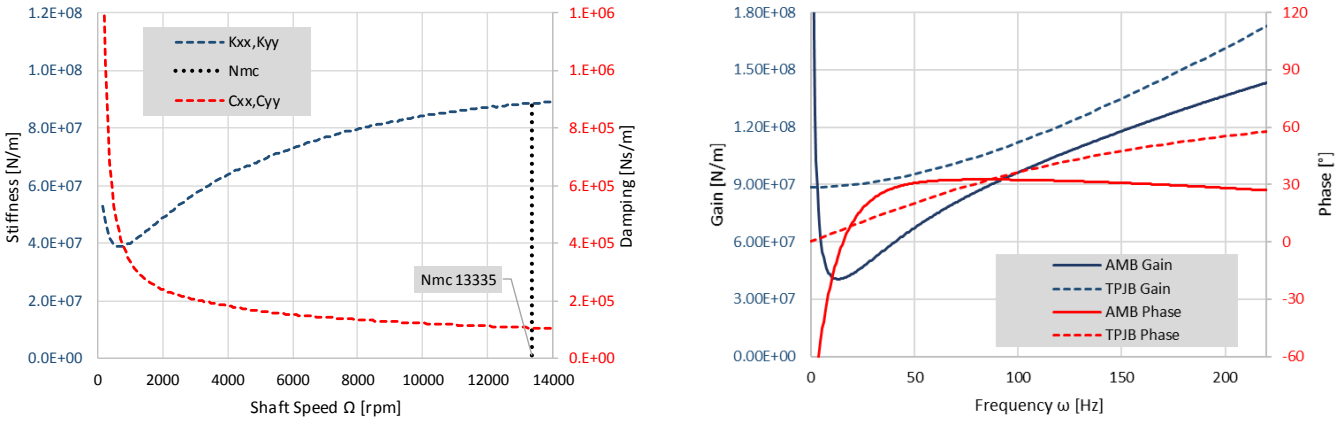

Figure 3: Comparison of Oil Lubricated and Active Magnetic Bearings Characteristics

Active magnetic bearings are less stiff than oil bearings. The oil bearing characteristics (dotted lines in Figure 3, right) are determined at 13335 rpm N_{mc} (vertical dashed black line in left plot), because API 617 prescribes stability screening at maximum operating speed, from the intersection of the black dotted maximum continuous speed line and the stiffness and damping lines. The AMB transfer function has a “gain hole” at low frequencies, which is typical for common industry PID shaped control designs. The minimum AMB gain at the gain hole is approximately half an oil bearing’s gain and in practice causes increased sensitivity to low frequency excitations.

An AMB can be susceptible to performance variation if the actuator and sensor air gap changes because of different rotor and stator temperatures and thermal expansion. For an oil-film bearing an overload can create high temperatures and higher stiffness before the oil-film collapses leading to a rotor stator contact. An AMB system will provide the required forces until reaching the bearing capacity limit, the shaft levitation and dynamic control is then lost. The touch down bearing system is designed to prevent harmful rotor/stator contact.

The low AMB stiffness is a drawback for high-density applications because seal gas forces are large and the AMB struggles to counteract the static and dynamic forces. Compressor fouling in upstream Oil and Gas operation causes additional gas forces and an adverse effect on the overall rotordynamic stability.

It is common that operators use vibration spectra as supporting measurement for the approach of the impellers stability line. Figure 4 shows a spectrum just at thermodynamic stability line (surge) during operation on a performance test (also part of normal FAT) of an AMB machine. The subsynchronous vibration is not visible only when the instability line (of impellers) is crossed, but well before. The higher observability helps operators to approach the surge line more consciously. On the other hand, the subsynchronous vibration generated by the disturbed pressure field leads to increased overall vibration signals and hence less margin to trip and alarm levels.

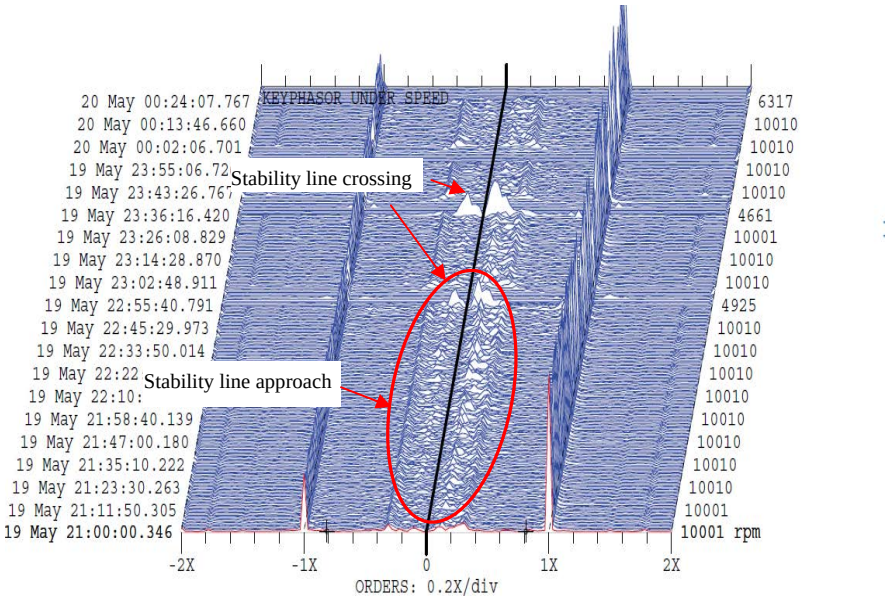

Figure 4: Measurement of compressor vibrations near surge for an AMB machine FAT

The complex frequency dependent AMB transfer functions inherent to the AMB rotordynamic model and software capability determine that equally complex labyrinth gas force models can be integrated into stability and unbalance response analysis with ease and therefore an API 617 Level II analysis is preferably performed. However, given the high AMB sensitivity to gas forces (low stiffness in low frequency region) and the large Level II gas force model (labyrinth stiffness and damping coefficients) uncertainty, the AMB compressor upstream application needs an improved stability screening method.

A displacement measurement feedback to the governing controller implies a new scenario: measurement noise does not only display on control room's screens, but generates a new force at the bearing. Hence, the layout of an AMB system must respect the full frequency range, while stability considerations for oil bearing machines concentrate on low frequency.

METHODOLOGIES FOR THE EVALUATION OF THE STABILITY BEHAVIOUR OF AMB-COMPRESSORS

API 617 Level I

Reliable centrifugal compressor stability behaviour evaluation requires accurate estimates of dynamic force characteristics for the bearings and all gas forces acting on the rotor (e.g. from labyrinth seals). However, the stiffness and damping model gas force model accuracy is still questionable despite the comprehensive analytical and measurements effort over the last decades. Kocur et. al (2007) show that depending on the OEM the same machine is theoretically stable or highly unstable and therefore the OEMs require a standardised compressor stability assessment procedure.

The first procedure step is the compressor Critical Speed Rigid Ratio (CSR: ratio between maximum continuous operating speed and first critical speed on rigid supports) to mean gas density characteristic and comparison in a diagram with known references. This diagram, introduced by Sood (1979) and further developed by Fulton (1984), includes a threshold line (see Figure 1) between historical stable and unstable machines and provides current compressor application stability severity assessment. In 2002 API 617 7th edition introduced a stability behaviour characterization methodology, a "Level I screening criteria". In addition to a stability map, split in two regions (A and B) based on the "Fulton-Line", a normalized destabilizing nonsynchronous force parameter Q_A is applied. This anticipated force is attributed to a cross-coupled stiffness and accounts for all labyrinth and impeller aerodynamic destabilizing forces. The Q_A parameter is a modified, empirical equation introduced by Wachel and von Nimitz (1981) that depends on the gas densities, impeller geometry, speed and power. API 684 describes the modified Wachel's equation. However, because of its simplicity, this method omits: (a) the gas force damping influence that improves stability, and (b) the gas force direct stiffness that influences the rotor natural frequencies. For flexible rotors with low bending mode frequency, the seal direct stiffness influence is important. Evans and Fulton (2010) provide the method's origin, application and the crucial flexible ratio (FR: ratio between maximum continuous operating speed and first forward mode) role. The crucial flexible ratio is influenced by the seal force direct stiffness and even a stiff rotor (low CSR) at moderate average density operation can become unstable with a negative gas force direct stiffness (which is realistic).

Swanson et. al (2014) provide background to the API 617 Level I and II analyses and the importance to consider the backward modes in addition to the forward modes. They state that the analysis should not be limited to the first mode, but all relevant modes with significant modal motion. This statement agrees with Smithanik and Paul (2015) who report that "the Level II analysis should be made initially, without considering the less detailed Level I".

Simplified Stability Evaluation

To increase compressor stability behavior assessment reliability it is necessary to weigh the different seal force effects together with the bearing properties. The behavior assessment can be simple or complex. For the simple Flexible Ratio (FR) method, a compressor equipped with AMB is more critical than oil bearings because the AMB bearing stiffness is much lower. Figure 5 represents the reference map for both oil and active magnetic bearings compressors.

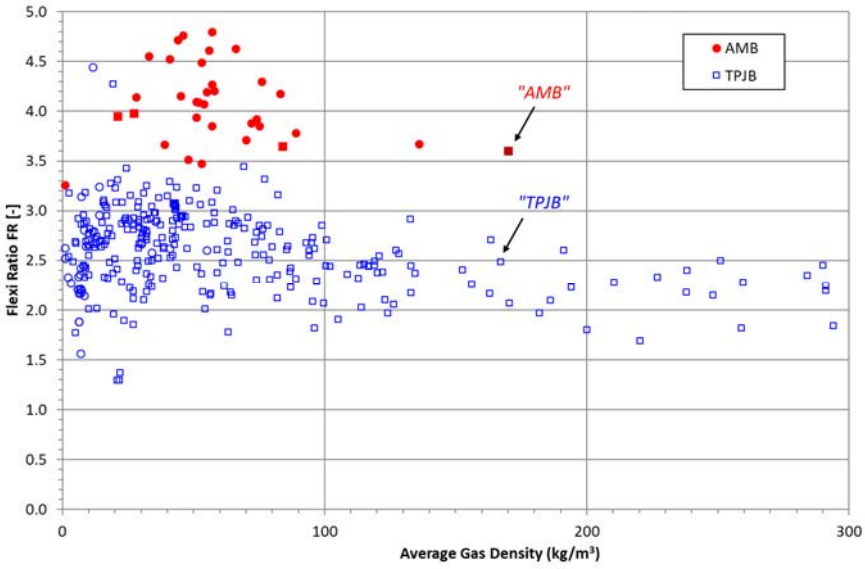

Figure 5: Flexible Ratio (unloaded) versus Gas Density with Centrifugal Compressor References

Baumann (2011) describes an alternative less simple method based on the ratio between the destabilizing and the stabilizing forces at each labyrinth seal (WFR_ω). Figure 2, right, illustrates how the labyrinth forces are modelled where, (a) the radial force F_{rad} is determined by the direct stiffness and cross-coupled damping, and (b) the tangential seal force F_{tan} is determined by the direct damping and cross-coupled stiffness.

The seal forces are stabilizing if the whirl frequency ratio based on the lowest whirling frequency is lower than 1, see Equation 4.

When the whirl frequency ratio based on the rotor speed (Ω) is compared to the *FR*, see Equation (5), a low FR allows higher destabilizing forces than a higher *FR*. Or, a low direct seal stiffness, or even negative direct stiffness, leads to a low first bending mode (high FR) and the stability threshold is then low and more sensitive to destabilizing forces.

$$WFR_\omega = \frac{K_{xy}}{C_{xx} \cdot \omega} \quad < \quad 1 \tag{4}$$

$$WFR_\omega = \frac{K_{xy}}{C_{xx} \cdot \Omega} \cdot \frac{\Omega}{\omega} \quad = \quad WFR_\Omega \cdot FR \quad < \quad 1 \tag{5}$$

API 617 Level II

The API 617 Level II analysis accounts for all sources contributing to the stability behaviour. The typical contributions are, (a) bearings, (b) labyrinth seals, (c) impellers (aerodynamic effects), (d) internal friction, and (e) oil bushings. High speed motors provide a special case because inherent motor negative electrical stiffness contributes to increase the FR. High circumferential speeds paired with a small air-gap can lead to significant interaction along the motor active length. AMB equipped machines provide additional contributions from gas forces in touch down bearing and actuator close clearance regions. The influence of the motor and AMB close clearance locations' gas dynamics grow with the local gas density. A typical fully sealed compressor train has motor and bearings surrounded by suction pressure.

The Level II analysis is at maximum continuous speed and is meaningful because the aerodynamic and fluid dynamic forces are highest and oil bearings deliver less damping and more stiffness at high speeds. API 617 specifies the analysis for the first forward mode only for oil bearing machines. For AMB equipped machines the analysis shall consider every mode up to twice speed frequency. Additional requirements state a maximum sensitivity transfer function of 3 according to ISO 14839-3 (Zone A). Swanson et al. (2014) published a more in-depth description of Level II analysis.

Motivation for Further Analysis

To ensure problem-free machine operation comprehensive computational efforts must be combined with sound component and machine design, which bases on extensive experience. The critical labyrinth seal operation influence is addressed by

- Seal type and geometry to reduce destabilizing gas forces.
- Seal inlet swirl conditioning devices to reduce inlet swirl velocity.
- Seal and impeller thermal deformation reduction by avoiding aggressive high operating temperatures.
- Differential pressure distortion reduction by rigid seal supporting structures.
- Impeller seal location deflection reduction by conservative speed and impeller type selection.
- Rigid shaft design to reduce vibration amplitudes at seal locations.

All the above points influence the seal clearance and it is the most important parameter that affects gas forces. Furthermore, the above points yield expensive machine configurations; therefore, the manufacturer and client shall reach a consensus to balance machine robustness, operational efficiency, and price performance.

The balance piston seal of choice for high pressure applications is a convergent clearance damper seal (hole pattern, honeycomb) because it provides high positive stiffness and damping. However, the damper seal application in AMB machines is difficult because the high positive stiffness creates high static forces and if the seal is eccentric to the AMB the resulting forces can reach the AMB capacity limit. The AMB can then not control the centered set point and the total bearing control is unstable. Furthermore, the strong damper seal gas force frequency dependency and variance depending on compressor operation create problems for robust AMB controller layout. Therefore, a lower gas force magnitude labyrinth balance piston is selected in AMB machines with drawback that this seal type has inherent negative direct stiffness.

The key uncertainty for the Level II analysis are the seal coefficients because their predictions are by far less reliable than the other elements of the rotordynamic system. The rotordynamic system elements are:

- The shaft(s)
- The bearings
- The coupling
- The seals

The shaft and coupling models are reliable and verified by bump tests if a new design. The oil bearing models are less reliable, but the prediction precision is acceptable. The magnetic bearing characteristics are reliable and predictable because AMB manufacturers know the sub-element (power amplifier, sensors, actuator) transfer functions by individual measurements.

If confidence in Level II predictions by the OEM or customer is not satisfactory, there are three approaches to raise the particular machine design confidence:

a) Establish restrictive thresholds, compared to common standards.
(Example: 0.2 log dec versus 0.1 as required by API 617)

b) Additional load cases calculations that cover particular risks
(Example: Prescribing additional sensitivity calculations for clearance, preswirl, or seal roughness)

c) A stability threshold search calculation with safety margin added to it.

Commonly, Oil and Gas industry specifications follow approaches a) and b) while structural analysis tasks follow c). An OEM will compliment these approaches with internal rules based on additional key figures with corresponding thresholds. For rotordynamic analysis an example is the Level I analysis search for Q_0 and its relation to Q_A.

The following sections focus on machine stability threshold evaluation by comparing operating machine stability reserves and then quantifying a planned new machine stability risk. For comparison, the supporting stability analysis calculations apply to candidate magnetic bearing and conventional oil bearing designs. After Level I and II analyses the approach c) stability threshold search applies an additional spring-damper element “K” to the base Level II loaded rotordynamic system (near surge operating conditions). The analysis applies near surge operation thermodynamic loads because the forces have the highest impact on the shaft compared to the Level I unloaded case. The location chosen for the additional spring-damper element is the piston. Piston location motivation stems from the high influence the piston has compared to other seals. A bearing midspan force location leads to similar results.

Figure 6 graphically summarizes stability related calculations and key figures. From top to bottom, the analytical model complexity increases with the integration of additional machinery elements. The colored rectangles represent suitable analysis for each rotordynamic modeling step with respective key figures shown on the top right edge (namely Critical Speed Ratio, Flexi-Ratio, cross coupled stiffness Q_0, the final log deg δ_f as well as the stability threshold values Q_{t0} and Q_{r0} discussed later). Dashed lines divide the regions into straight forward versus parameterized analysis types.

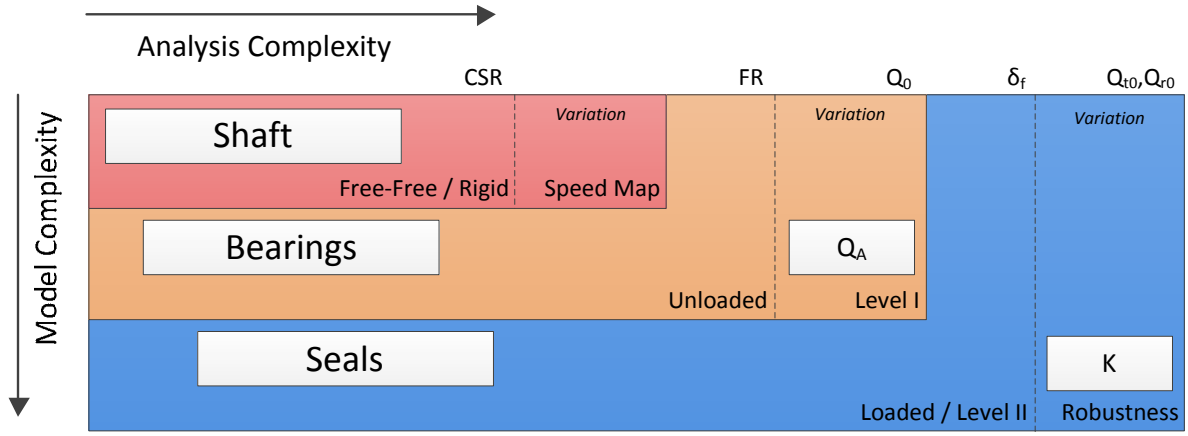

Figure 6: Analysis schematics

ONE COMPRESSION DUTY, TWO COMPRESSOR DESIGNS

Representative AMB and an existing “conventional” TPJB (Tilting Pad Journal Bearing) high pressure compressor design stability analyses form a comparison basis. The existing TPJB compressor is in operation since 2007 without problems.

Table 2: Key features of compressors.

Feature	Units	AMB Compressor	TPJB Compressor
Number of Stages	#	7	6
Tip Diameter	mm	400	300
Suction Pressure	bara (psi)	83 (1204)	95 (1380)
Discharge Pressure	bara (psi)	321 (4656)	331 (4801)
Average Gas Density	kg/m^3	170	167
Discharge Gas Density	kg/m^3	222	219
N_{mc}	rpm	10606	13335
CSR	-	1.2	2.1
FR	-	3.6	2.5
Anticipated Q_A	N/µm	7.3	10.8

Both compressors have similar operating conditions (see Table 2) and are designated AMB and TPJB in the following figures. The shaft speed is different because different design philosophy and constraints apply between oil bearing and sealed high-speed motor solutions and therefore the size and number of impellers differ to reach the pressure ratio. Table 2 lists a compressor key features comparison. Because the production mass flow rate is higher, the TPJB machine operates with higher power. However, the main difference is the overall shaft design, the number of bearings, and the AMB rigid-coupled high-speed motor to compressor shaft. Figure 7 shows a comparison of the relevant shaft models and identifies bearing (blue triangles), gas force elements (green labyrinths), and additional spring/damper elements (blue spring dashpot) locations.

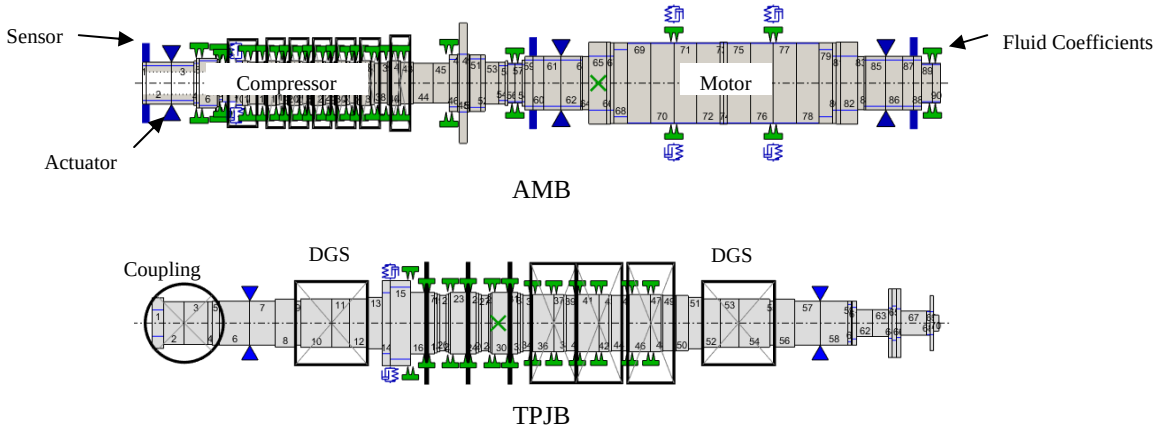

Figure 7: Mass elastic models for the rotordynamic calculation

The sealed motor operates at near compressor inlet conditions and has both electromagnetic radial negative stiffness (spring) and gas forces in the air-gap. The AMB machine includes additional gas force producing elements at the close clearance touch down bearing locations. Sets of fluid coefficients (stiffness and damping) model the gas forces (green labyrinths) for motor and for compressor. The TPJB machine has a standard shaft configuration including Dry Gas Seals (DGS), a thrust bearing collar and a flexible coupling. Despite rather high discharge pressure levels, both machines have see-through stationary teeth labyrinth at impeller and balance piston seals.

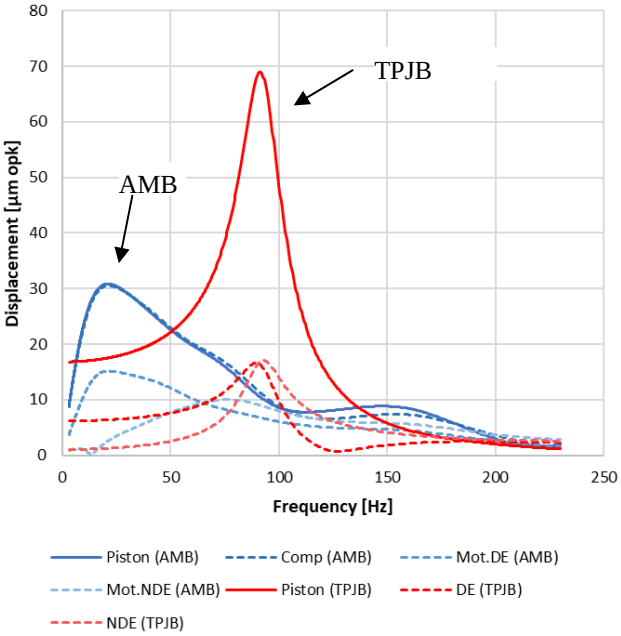

Figure 8: Comparison of response to asynchronous force excitation at N_{mc}

An asynchronous harmonic force excitation analysis reveals the different bearing dynamic characteristics effect combined with the two particular shaft designs. Figure 8 compares the AMB compressor versus “conventional” TPJB (Tilting Pad Journal Bearing) compressor displacement response for a 1000 N radial force injection at the balance piston. Displacement evaluation at the balance piston eliminates rotor bending shape effect between piston and displacement probe. The AMB compressor response (blue curve in Figure 8) follows an inverse gain hole characteristic and creates a vibration peak at low frequency. The TPJB machine first bending mode vibration peak is at approximately 90 Hz. In contrast, the AMB compressor high effective damping on the bending mode (crossed at 150 Hz) suppresses the resonance response. The high AMB mode damping ability is only possible when the corresponding rotor mode shape has high modal deflection at the bearing location and this is the case for rigid coupled motor-compressors. Additionally, Figure 8 shows the displacements at sensor locations where it is noted that the AMB compressor bearing sensor response follows the piston but the oil bearing machine does not. If a piston location aerodynamic flow disturbance occurred at 25 Hz a machine operator will view (sensor signals only) a 97% (31µm/32µm) piston response for the AMB compressor compared to 39% (7µm/18µm) piston vibration response for the oil bearing compressor. Hence, the AMB compressor piston seal deflection is well observable because the shaft section between radial sensor and piston seal is stiffer.

STABILITY ANALYSIS

Level I Analysis

API 617 Level I is an eigenvalue analysis for both unloaded and cross-coupled stiffness loaded shaft systems. Figure 1 shows both machine designs CSR versus average density characteristics and note that the average density is well above 60 kg/m^3. Therefore, both machines are in Region B.

The criteria in API 617 apply to both machines below maximum continuous speed. Conventional TPJB compressors evaluate the first forward mode but AMB compressors all forward modes up to twice maximum continuous speed (API 617, Annex E). The frequency dependency criteria in Annex E require modal frequency (N_{mode} in rpm) collection in addition to the loaded system (δ_A) damping and the destabilising cross-coupling Q_0/Q_A ratio.

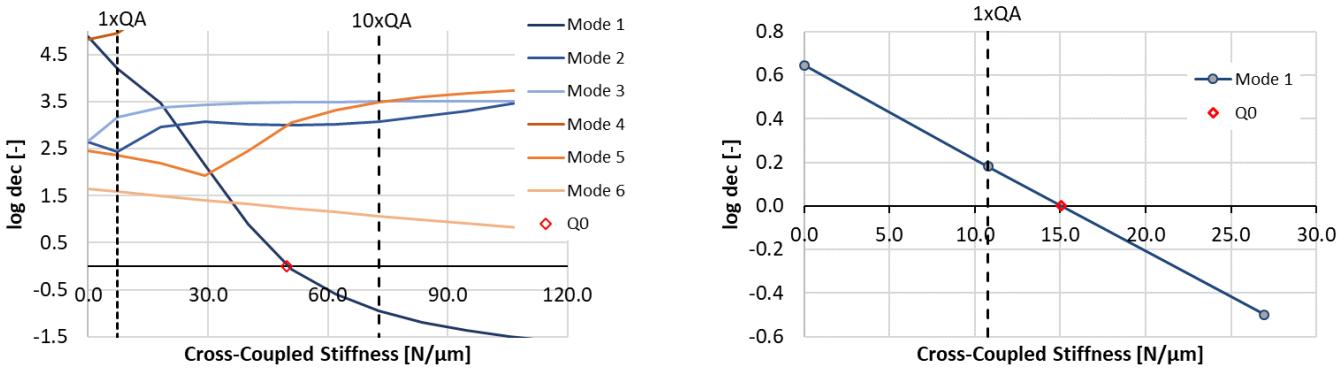

AMB (Q_0=6.8x Q_A) TPJB (Q_0=1.4x Q_A)

Figure 9: Results for the varying amount of cross-coupled stiffness as per API 617

Figure 9 shows on the left the AMB and on the right the TPJB API 617 Level I analysis results according to the eigenvalue calculations for an unloaded and cross-coupled loaded shaft bearing system. Table 3 summarizes the Level I analysis results with a criteria conformance list and highlights (red "yes") when a Level II analysis is required.

Table 3: API 617 Level I key figures

TPJB	Calculated			Level I Criteria				
§ general Section				4.8.5.8-1	4.8.5.8-2	4.8.5.8-3		
Mode	N_{modeA}	δ_A	Q_0/Q_A	$Q_0/Q_A < 2$	$\delta_A < 0.1$	$(Q_0/Q_A<10)$ & (B)		
	[rpm]	[-]	[-]	[y/n]	[y/n]	[y/n]		
#1	5535	0.13	1.4	**yes**	no	**yes**		
AMB	Calculated			Level I Criteria				
§ in Annex E (AMB)					E.4.8.5.2 b)		E.4.8.5.2 c,d)	E.4.8.5.3
§ general Section				4.8.5.8-1	4.8.5.8-2	4.8.5.8-3		
Mode	N_{modeA}	δ_A	Q_0/Q_A	$Q_0/Q_A < 2$	$\delta_A < 0.1$	$(Q_0/Q_A<10)$ & (B)	$\delta_A > f(N_{mode})$	Gs < 3
	[rpm]	[-]	[-]	[y/n]	[y/n]	[y/n]	[y/n]	[y/n]
#1	1108	4.43	6.8	no	no	**yes**	no	
#2	907	2.20	>10	no	no	no	no	
#3	2313	5.12	>10	no	no	no	no	
#4	4330	2.39	>10	no	no	no	no	no
#5	9383	1.59	>10	no	no	no	no	
#6	17408	0.72	>10	no	no	no	no	

The AMB machine Level I stability assessment is more elaborate because every mode in the range from 0 Hz to double the maximum continuous speed is analysed. Annex E states the three Level I criteria, in the general section of API 617, application to the modes.

Figure 9, left, shows that only mode #1 is driven unstable by the applied cross-coupled stiffness and the stability threshold is at cross-coupling ratio 6.8. All AMB cross-coupling ratios are larger than 2 (API 617 – Level I Criteria). Because AMB Mode 1 has Q_A/Q_0 less than 10 and is in region B, the first mode fulfils the Level I criteria of API 617 and a Level II analysis is required.

Figure 10, left, shows log dec versus normalised mode frequency for all AMB frequencies, f(N_{mode}), with the API 617 acceptance criteria, governed by Annex E, as a dashed line.

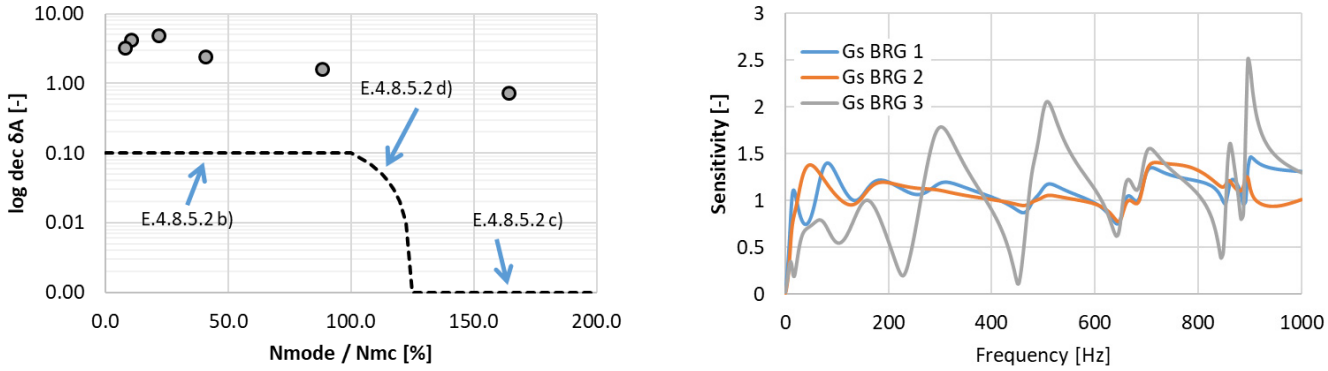

Figure 10: Level I Analysis add on for AMB units: Log dec (left) and Sensitivity Analysis (right) acc. to Annex E

The AMB Level I also requires a system sensitivity function check with 2 x Q_A and the sensitivity shall not exceed a value of 3 (ISO 14839-3 Zone A). Figure 10 (right) shows that the corresponding AMB system sensitivity does not exceed 2.5.

The Level I analyses determine that Level II analyses are required for both machines because, (a) the AMB machine meets the cross-coupling ratio ($Q_0/Q_A < 10$) and the "Region "B" criteria, and (b) the TPJB machine meets the ($Q_0/Q_A < 2$) criteria. The TPJB machine appears more critical because it would need a Level II analysis if compressor operation would be in "Region A".

If backward modes are considered, the Level I analysis results remain the same because the backward mode shapes are similar to the forwards.

Level II Analysis

A Level II analysis expands on Level I to include the seal coefficients. Figure 11 shows that both AMB (lines) and TPJB (dots) machines are stable for various loaded conditions and Figure 12 shows the AMB machine sensitivity remains within ISO 14839-3 zone A. The various loaded conditions address compressor operation (surge and choke), condition (rough), and seal geometry (clearance) effects and are compared with the reference unloaded (red line and dots) case.

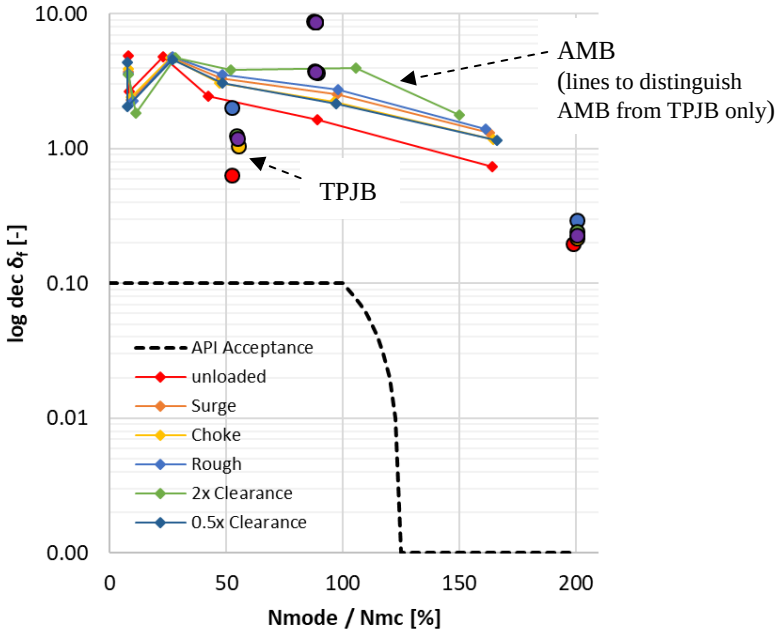

Figure 11: Stability Spectrum for Level II Analysis

The AMB machine has six forward modes in the frequency range of interest (200% maximum continuous speed). The TPJB unit has four forward modes, presented for completeness. Both machines have stabilizing seal forces for frequencies above 25 % of maximum continuous speed. The AMB machine has modes at lower frequencies with less damping than the unloaded base case (red line). The tangential force study, presented in chapter "Simplified Stability Evaluation", shows that it is more difficult to stabilize the system at lower eigenfrequencies because the FR increases and increases the WFR_{ω} (Equation 5) over 1.

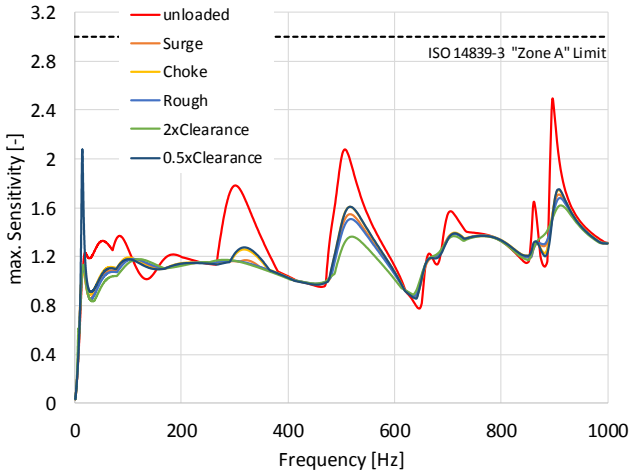

Figure 12: Sensitivity functions for the loaded conditions.

The seal damping coefficients have little overall stabilizing effect at low frequencies because the damping force is the product of the coefficients with the low frequency and yields a small stabilizing force (ωD_{xx}). Hence, cross-coupled stiffness determines rotor stability. A later section on seal coefficients provides a detailed discussion on seal frequency dependent effects and stabilization.

Figure 12 shows the maximum of the three AMB sensitivity functions for the rotor running at maximum continuous speed. Small clearances lead to a sensitivity peak at low frequency exceeding the unloaded (red line) baseline. Otherwise, the seals reduce the machine's sensitivity to AMB feedback alterations at each peak.

The Level II analyses for both machines fulfil the required stability margins and hence, no machine operational problems are expected.

Robustness to Cross-Coupled Stiffness

Figure 13 shows, analogous to Level I, an added cross-coupled stiffness variation analysis applied at the balance piston for both machines where negative and positive cross-coupling is increased to destabilize both the backward and forward modes. This cross-coupled stiffness is added to the surge region operation loaded conditions (black lines, Level II base case).

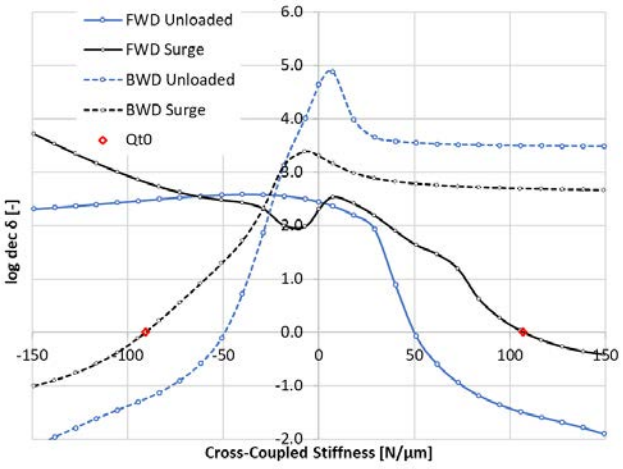

AMB

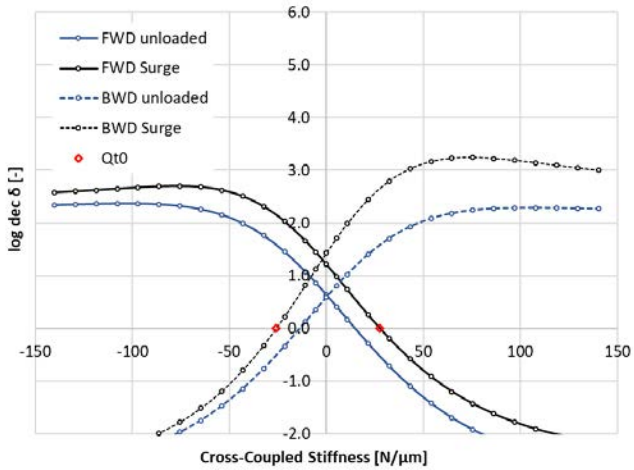

TPJB

Figure 13: Variation of cross-coupled stiffness for the unloaded case and the loaded case at surge conditions.

In addition the same stiffness is applied to the unloaded condition (blue lines), for comparison to Level I. The cross-coupled stiffness magnitude needed for destabilization is identified by Q_{t0} (red symbol) and is lower for the backward mode than for the forward modes in all cases.

The seal forces stabilizing effect from the Level II analysis translates to higher stability thresholds compared to the unloaded analysis. The cross-coupled stiffness is quantified in absolute values to compare AMB versus TPJB shaft and shows that the AMB machine tolerates higher cross-coupled stiffness for all modes and conditions.

Figure 14 compares the AMB versus TPJB machine mode shapes first hitting the stability threshold at ω_{t0} and shows, via an arrow, the respective cross-coupling force injection location. The TPJB machine mode shape shows high modal deflection at the seal locations and low deflection at the bearings, which is the reason why the Q_{t0}/Q_A ratio is lower than the AMB machine that has high modal damping contribution from high modal deflection at the bearings.

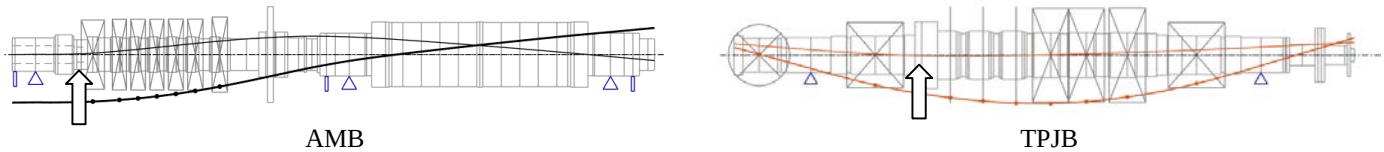

AMB TPJB

Figure 14: First unstable forward mode shapes at stability threshold ω_{t0}

The additional cross-coupling on the system changes both the damping and the frequency. While Figure 13 shows the influence on the damping only, Figure 15 presents both modal frequency and damping for the forward and backward mode of the TPJB machine in near surge condition operation. For the system without additional cross-coupled stiffness, marked with grey dots, negative cross-coupling moves the mode towards the blue crosses, and positive cross-coupling moves the modes to the red crosses. The zero log dec at Q_{t0}, denoted with small red diamonds, has the frequency ω_{t0} where the mode becomes unstable. The ratio Q_{t0}/Q_A provides a means to compare the margin to stability threshold and for the AMB machine the ratio is superior at 13.7 versus 2.6 for the TPJB machine.

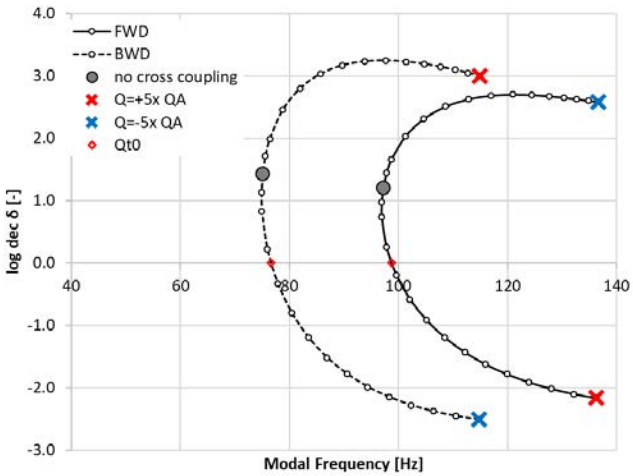

TPJB

Figure 15: Mode path as function of cross-coupled stiffness (loaded at surge condition)

The cross-coupled stiffness variation showed corresponding eigenfrequency variation; however, a radial direction force from direct stiffness will cause greater eigenfrequency variation and potential to lower the eigenfrequency with increased sensitivity destabilizing cross-coupled forces.

Robustness to Direct Stiffness

To investigate the radial force influence on the rotordynamic stability a direct stiffness variation is applied in the same manner and location, piston seal, as the previous cross-coupled stiffness variation: it is added to the surge region operation loaded conditions (Level II). Figure 16 compares the AMB versus TPJB machine least stable mode damping from direct stiffness variation. It shows that increased negative direct stiffness always reduces AMB machine stability but increases TPJB machine stability until the backward mode eigenfrequency reaches 0 Hz, causes a singularity, then is an unstable mode at -55 N/µm. Camatti et al. (2003), Eldridge and Soulas (2005) and Moore et al. (2006) report that a divergent clearance seal caused rotordynamic instability. All cases show that the divergent clearance develops strong negative stiffness that destabilizes a low frequency mode consistent with the pattern shown in Figure 16 right side.

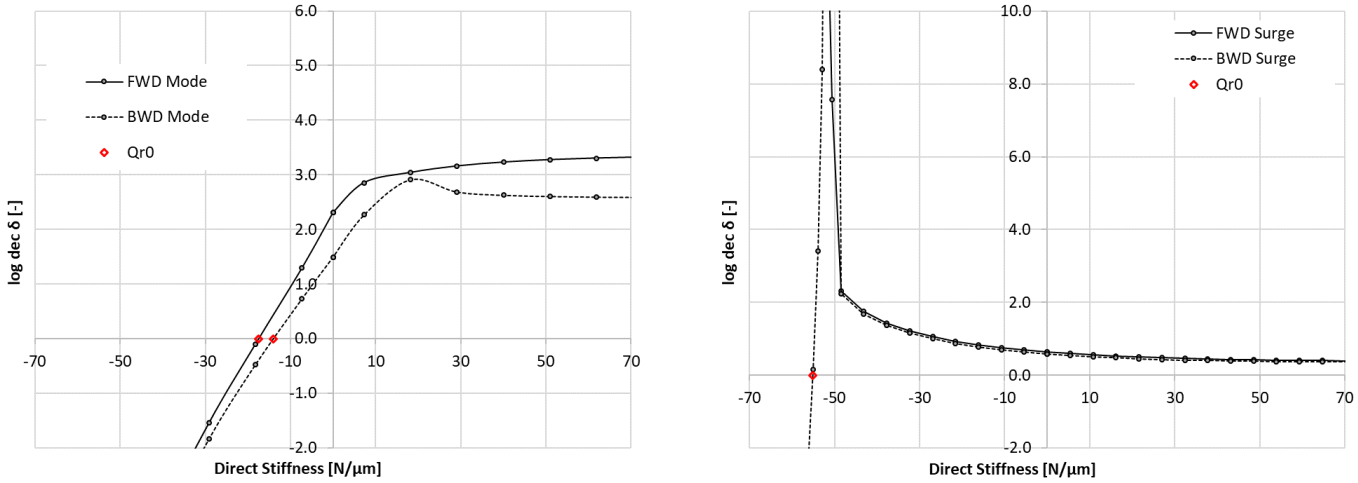

AMB TPJB

Figure 16: Variation of Direct Stiffness (both in positive and negative direction) loaded at surge conditions.

The ratio of negative direct stiffness to the anticipated cross-coupled stiffness, Q_{r0}/Q_A, is an inferior -2.2 for the AMB machine and -5.1 for the TPJB machine. Therefore, the AMB machine shows higher sensitivity against the radial force compared to the TPJB machine. Figure 17 compares the AMB versus TPJB machine mode shapes at Q_{r0}. The TPJB machine mode shape (right) is the same shape as at Q_{t0} in Figure 12, but the AMB mode shape (left) has a cylindrical form with all bearings at the same phase. The threshold frequency for the AMB machine instability, ω_{r0}, is 17.2 Hz versus 10 Hz for the TPJB machine.

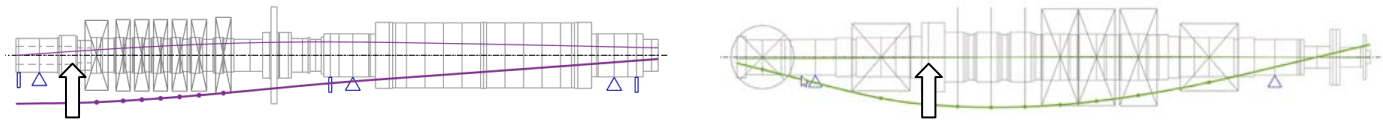

AMB (FWD) TPJB (BWD)

Figure 17: Mode shape at Q_{r0}

The direct versus cross-coupled stiffness variation yields contrasting stability results because, (a) the AMB machine is less sensitive to cross-coupled stiffness variation but sensitive to direct stiffness variation, and (b) the TPJB machine is sensitive to cross-coupled stiffness variation but less sensitive to direct stiffness variation. Hence, it is not obvious which stiffness parameter is most adverse; therefore, the next section investigates a variation of a general force that is a combination of the two stiffness parameters.

Robustness to Generalized Force

A direct and cross-coupled stiffness combination provides a generalized force with direction influence on the shaft systems. Applying a gain/phase force representation facilitates force parameterization and covers all radial force directions and worst force angle (phase) determination. Figure 18 shows the generalized force model.

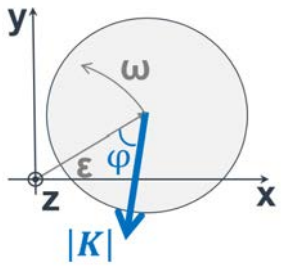

$$\begin{bmatrix} K_{rad} \\ K_{\tan} \end{bmatrix} = \begin{bmatrix} \cos(\varphi) \\ -\sin(\varphi) \end{bmatrix} K$$

K_{rad} = Direct Stiffness

K_{tan} = Cross-Coupled Stiffness

Effect for main phases φ:

0° = positive stiffness

90° = positive damping

180° = negative stiffness

270° = negative damping

Figure 18: Planar parameterization of the added spring

With the Level II model as basis, the calculation procedure applies additional gain (K) followed by angle (φ) variation from 0 to 360° sequences to form concentric increased gain, from 0.5 to 5 Q_A, generalized force calculation sets. The analysis applies the generalized force at the same (piston) location. For each calculation in each set, the least damped mode's damping ratio (modal damping) and eigenfrequency is extracted and stored. Figure 19 shows the results of all calculations for the TPJB machine. The plotted data uses 13

color-coded gains to show sensitivity to stiffness “circles”. Modes with high stiffness sensitivity have high scatter. Figure 19 extends Figure 13 presentation to include both radial and cross-coupled stiffness effects (dashed black lines for the most sensitive mode).

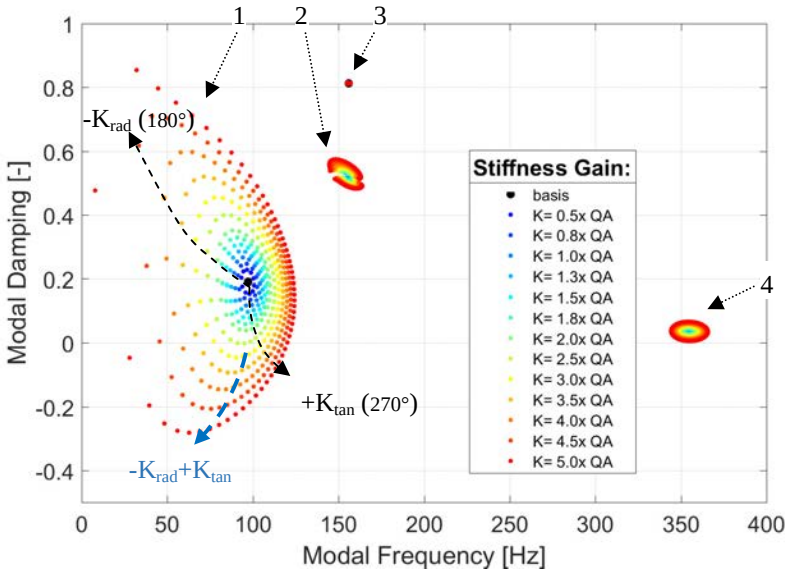

Figure 19: Stiffness Circle parameter variation (TPJB Machine, up to 5xQA), Forward modes

The most sensitive mode is the first forward mode labeled with “1”. Note that the 0 modal damping line intersects the stiffness circle directly below (phase -90°, positive cross-coupled stiffness) the basis point with a light green (K = 2.5 x Q_A) coded K magnitude and confirms consistency with the TPJB machine Q_{t0}/Q_A = 2.6 pure cross-coupled stiffness variation results above. The negative direct stiffness direction is labeled with $-K_{rad}$ and, when combined with a positive cross stiffness, produces the most unstable force direction (dashed blue line). Figure 19 also shows additional less sensitive modes, (a) a coupling overhang mode (“2”) at 160 Hz, (b) an axial bearing overhang mode (“3”) at 155 Hz and (c) the second bending mode (“4”) at 360 Hz.

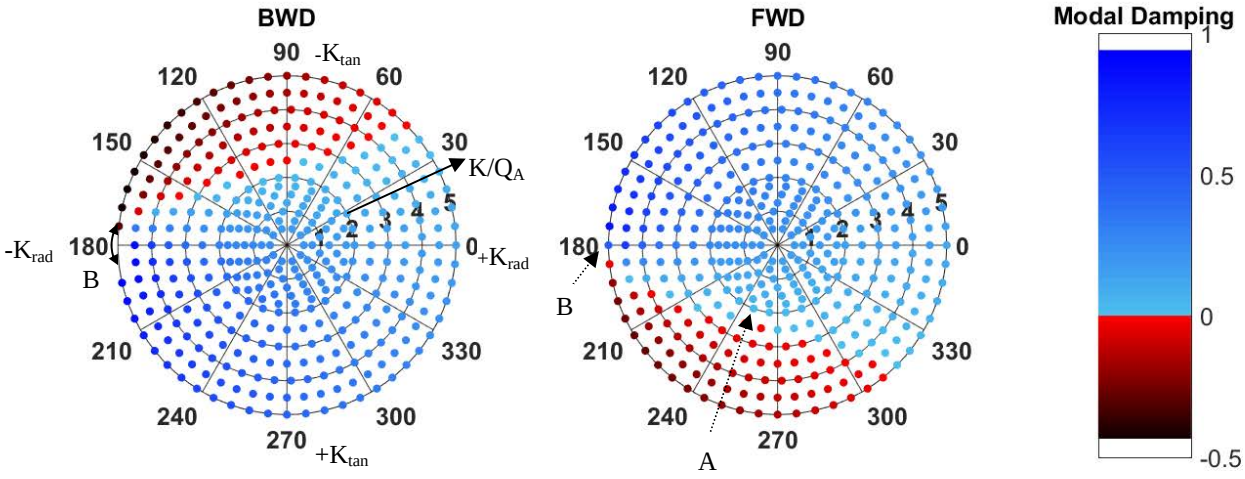

Figure 20: Polar plot of parameters, color-coded modal damping (TPJB machine)

Figure 20 shows the TPJB machine gain and phase variation parameter results, for the 1st bending (most sensitive) backward (left) and forward (right) modes, in a polar plot with color-coded resultant modal damping. The color coded modal damping is blue for stable and red for unstable modes and the intensity, light to dark, shows the low to high modal damping level. The vertical axis (90° to 270°) is the sensitivity to cross-coupled stiffness (K_{tan}) and the horizontal axis (0° to 180°) is the sensitivity to direct stiffness (K_{rad}). The red points in the left plot show that the backward mode is unstable in the upper (negative K_{tan}) region and on both left and right, but weighted more to the left (negative K_{rad}). The forward mode plot (right) shows similar characteristics but in the lower region where K_{tan} is positive. Points “A” and “B” identify respective modes that are at instability threshold for forward and backward modes and

both points correspond to the same stiffness magnitude (K = 2.5 x Q_A) shown above.

The AMB machine results are more complex because more modes are involved. Figure 21 shows the AMB machine modal damping versus modal frequency for an extended stiffness range. Note that compared to the TPJB machine, modes merge depending on the added stiffness, K, gain and phase. The sub plot on the right provides narrower modal damping range to better identify the low frequency modes.

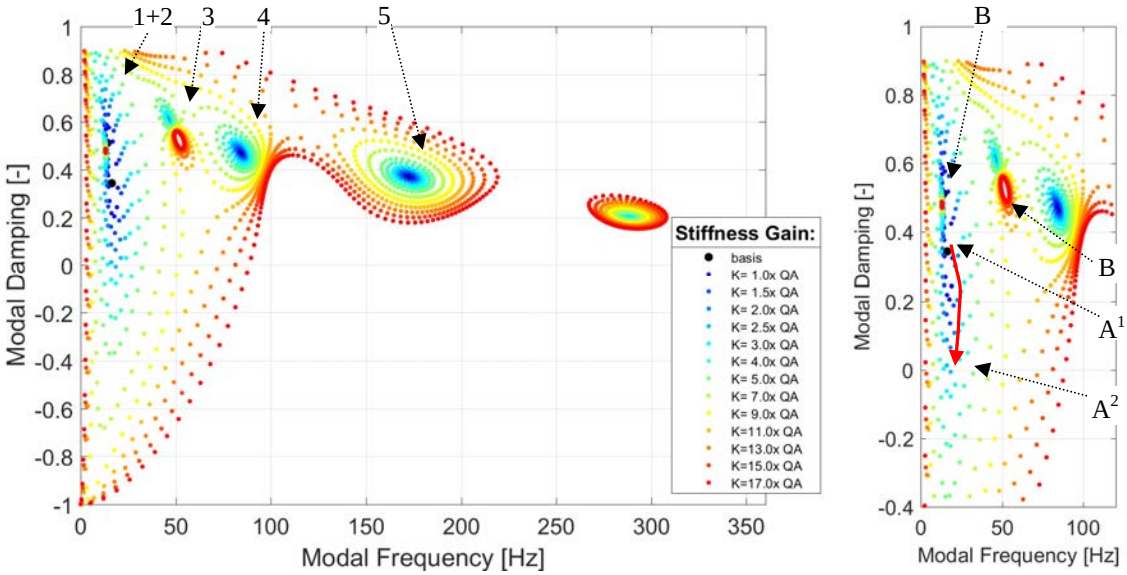

Figure 21: Stiffness Circle parameter variation (AMB machine up to 17.0xQ_A), Forward Modes

There are five modes below 200 Hz in the left plot and identified as, (a) rigid rotor Modes 1 and 2 that are dominated by motor negative stiffness, (b) conical rigid rotor Mode 3, (c) a rigid rotor like compressor versus motor rotor tilting Mode 4 and (d) the overall rotor bending Mode 5. The low frequency modes are most interesting and an increased gain trajectory (red line) shows the initial point "A^1" to first instability at "A^2" that occurs with a light green color code (K = 5 x Q_A).

The highlighted locations "B" show two confined zones where the modes frequency converges when the gain increases. Mode 1 and Mode 3 remain well damped for arbitrary stiffness gains K.

Figure 22 shows the corresponding AMB machine variation of gain and phase parameter results for the most sensitive backward and forward modes. The distinct red dots on left side results confirm the previous AMB machine findings that negative direct stiffness causes the initial instability for both backward and forward modes. The outermost circle at 17.0xQ_A shows that the AMB also is unstable with pure cross-coupled stiffness (90° for the backward mode and 270° for the forward).

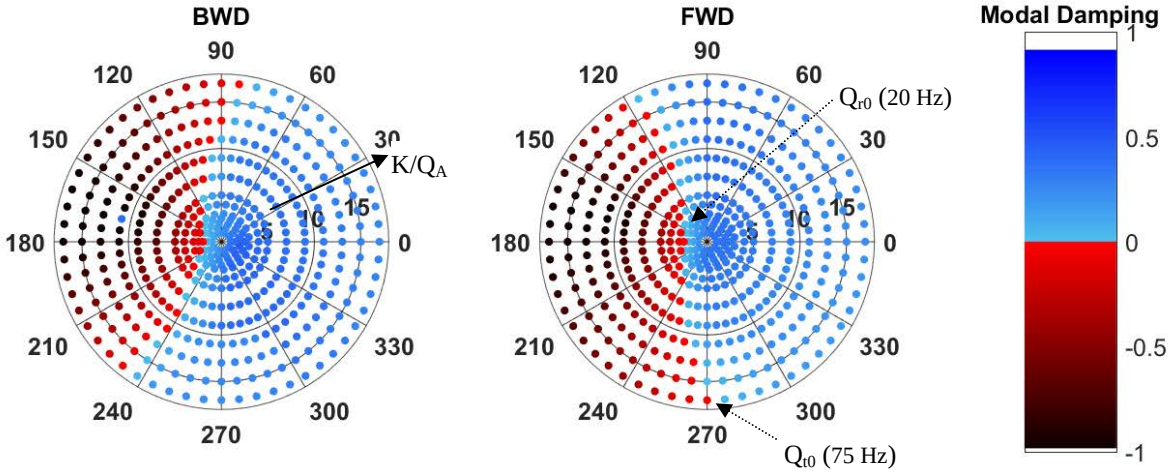

Figure 22: Polar plot of parameters, color-coded modal damping (AMB machine)

The above results reveal the contrasting TPJB versus AMB machine rotordynamic stability characteristics; an AMB machine is destabilized first by pure negative stiffness but a TPJB machine by cross-coupled stiffness. Table 4 summarizes the forward and backward mode margins for AMB versus TPJB comparison.

Table 4: Stiffness variation key figures

				AMB		TPJB	
				BWD	FWD	BWD	FWD
	Variation	Q_A	[N/µm]	7.3		10.8	
Unloaded	Cross-Coupled	Q_0 / Q_A	[-]	-6.7	6.8	-1.3	1.4
Loaded	Cross-Coupled	Q_{t0} / Q_A	[-]	-10.8	13.7	-2.4	2.6
	Direct	Q_{r0} / Q_A	[-]	-1.6	2.2	-5.1	-
	Gain / Phase	K_0 / Q_A	[-]	1.6	2.2	2.4	2.5
		φ_0	[°]	175	180	105	255

Tangential and radial parameterized stiffness studies describe satisfactorily the safety factors to stability thresholds for loaded compressors and suffice to categorize a machine: the worst-case phase angle found for the additional stiffness gain is near to the parameter variation of added cross-coupled stiffness (TPJB) and added direct stiffness (AMB). A full gain/phase parametrisation contains additional information valuable to understand systems stability threshold behaviour.

Selected Harmonic Analysis

Figure 23 shows the AMB machine sensitivity transfer function calculations for varying stability threshold Q_{t0} (left) and Q_{r0} (right) levels compared with both unloaded and basis (Level II at "surge") conditions. The left sensitivity plot shows that the AMB machine exceeds Zone A limit sensitivity for the 80 Hz mode with tangential force near the threshold level. In contrast, the right sensitivity plot shows steady increased sensitivity for both backward (10 Hz) and forward (20 Hz) low frequency modes to a radial force and exceeds the Zone A limit at 0.5 to 0.75 threshold level.

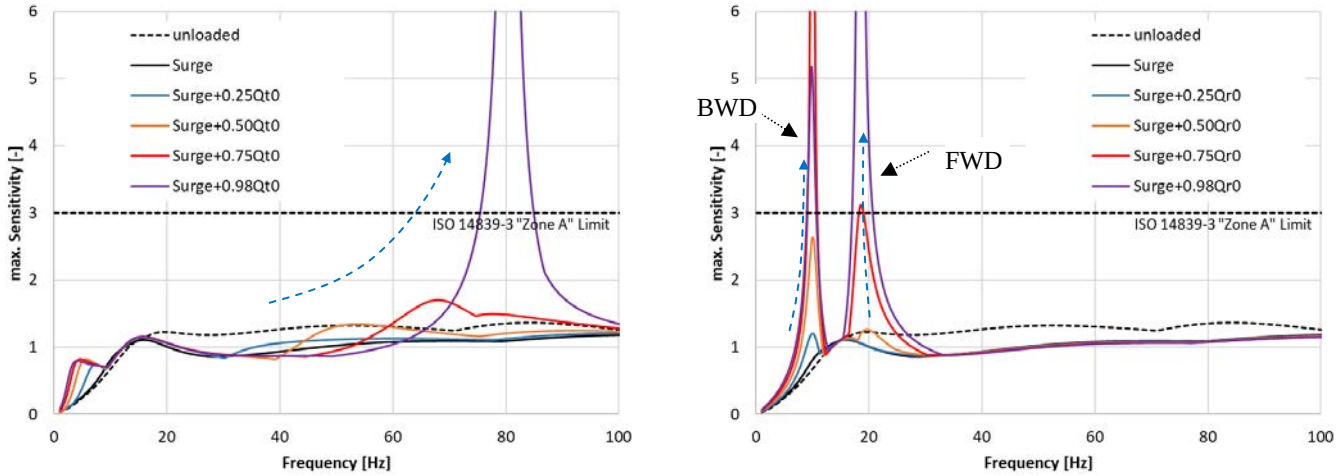

Figure 23: Evolution of Sensitivity Function when approaching stability thresholds Q_{t0} (left) and Q_{r0} (right)

The lower peak on the backward mode at 98% compared to the red line for the 75% is due to the mathematics of the response analysis's amplification function. Additionally Annex A will discuss non-synchronous excitation force response for both the TPJB and the AMB machines.

SEAL COEFFICIENT VARIATION STUDY

The comprehensive rotordynamic stability calculations presented include Q_A ratio safety margins for both compressor types (TPJB and AMB); however, because there is additional seal force uncertainty a seal coefficient uncertainty margin is needed.

To assess the seal coefficient uncertainty, selected representative machine (identified from 1 to 6) analyses, with different gas density categories, provide lower and upper uncertainty bounds. Table 5 shows compressors 1 to 6 density and pressure operating conditions. Labyrinth seal types, see-through stationary teeth at the impeller labyrinth seals, and stepped stationary teeth at the balance piston seal, subjected to parameter variations, provide labyrinth seal coefficient sets for each machine. The parameter variations are:

a) Dry operation influence between surge and choke at maximum continuous speed,
b) 10x design roughness on labyrinth stator and rotor surfaces,
c) Increased clearances (2x nominal value),
d) Divergent and convergent piston seal clearances (½ nominal clearance for minimum value).

Table 5: Key figures of operating conditions for compressors 1 to 6

Compressor		N_{mc}	Average Density	Suction Pressure		Discharge Pressure		Flexi Ratio	Cross-Coupling Q_A
		[rpm]	[kg/m^3]	[bar]	[psi]	[bar]	[psi]	[-]	[N/µm]
#1	AMB	10606	170	83	1204	321	4656	3.6	7.3
#2	TPJB	13335	167	95	1378	331	4801	2.5	10.8
#3	other TPJB machines	13335	135	71	1030	201	2915	2.4	8.0
#4		11180	95	70	1015	180	2611	2.1	4.5
#5		13317	65	20	290	126	1827	3.0	8.6
#6		18794	42	20	290	66	957	2.9	2.3

Figure 24 shows the cumulated parameter variation influences a), b), c), normalized to the basis surge conditions, on the resultant stiffness and damping coefficients for all seals. The coefficients most sensitive to the parameter variation are the tangential force component cross-coupled stiffness (blue) and direct damping (red) coefficients. The figure also shows the additional convergent and divergent clearance piston seals influence, d) and note that the relative change (to surge basis) further increases. Table 6 summarizes the parameter variation extreme stiffness and damping coefficient relative changes and defines the seal coefficient uncertainty boundaries for the six compressors listed above.

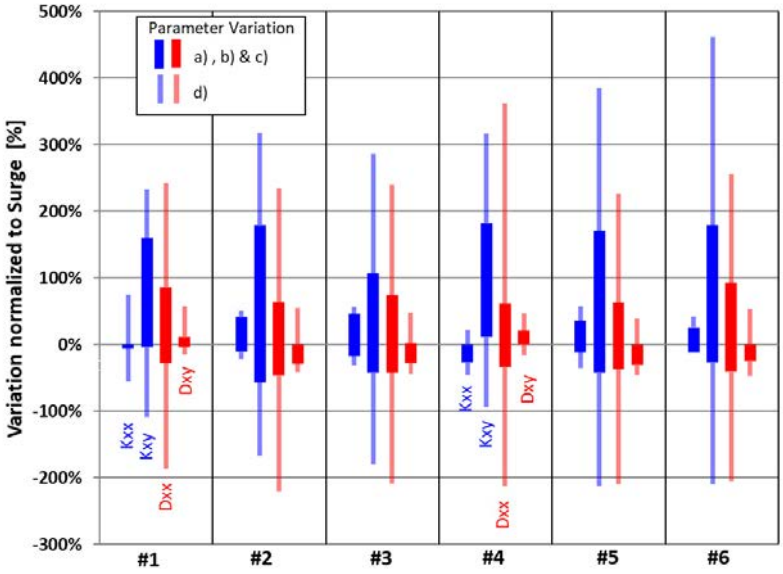

Figure 24: Normalized Seal coefficient variation candle plot

The upper and lower seal coefficient uncertainty bounds in Table 6 are collected to form radial and tangential impedances, F_{rad}/A and F_{tan}/A in Equation 2, and these impedances form the seal uncertainty zone boundaries and are normalized with respective AMB and TPJB Q_A values. Two seal coefficient uncertainty zones are formed for each machine, one from seal parameter variations a), b) and c), and one from convergent/divergent piston clearance variation parameter d). The uncertainty zones are conservative because the individual coefficient extremes are collected independently to the individual parameter variation source and yields wide zones.

Table 6: Normalized seal coefficients maxima and minima

		Kxx	Kxy	Dxx	Dxy
Surge, Choke, Rough 2x Clear.	Lower bound [%]	-25	-55	-45	-30
	Upper bound [%]	45	180	90	20
Divergent/Convergent	Lower bound [%]	-55	-210	-220	-50
	Upper bound [%]	75	460	360	60

Figure 25 compares the AMB (left) and TPJB (right) radial and tangential force variation stability analyses with the respective seal coefficient uncertainty zones (dark gray: zone for load variation, roughness and clearance wear, light gray: with additional convergent and divergent balance piston seal clearance). Both the backward and forward modes merge into a single polar plot.

Note that the tangential force components (vertical axis) dominate the elliptical shaped uncertainty zones. The distance between the nearest unstable point (red dots) to the seal uncertainty zone provides the seal coefficient uncertainty margins and for the AMB machine it is 1.5 Q_A and for the TPJB machine it is 0.5 Q_A.

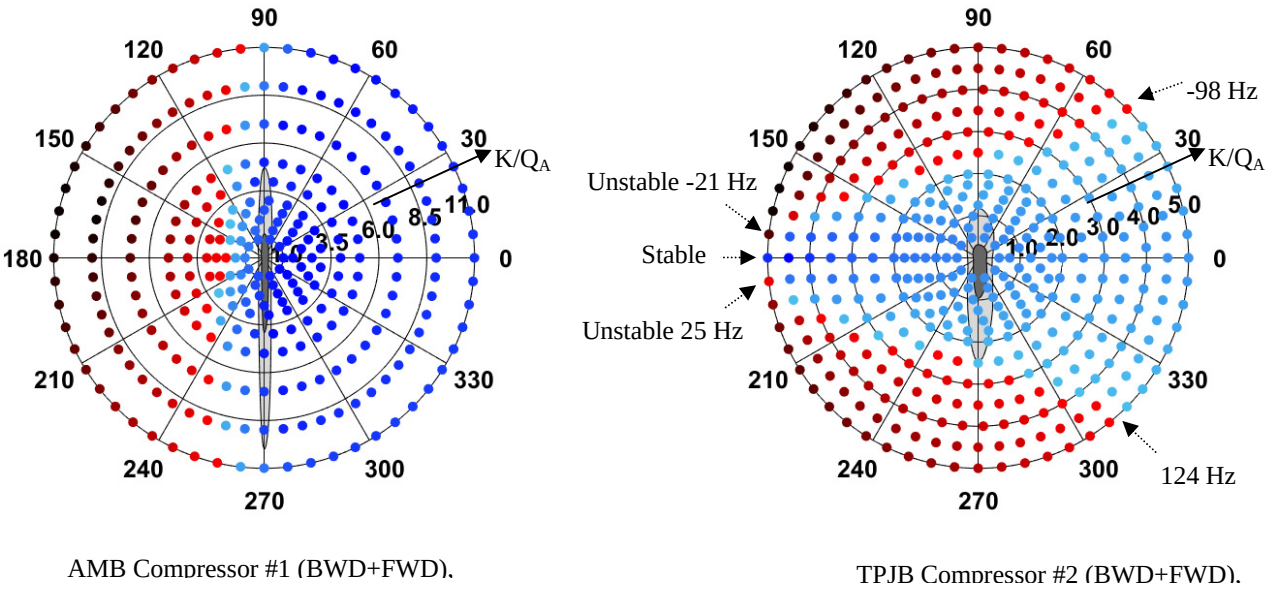

AMB Compressor #1 (BWD+FWD).

TPJB Compressor #2 (BWD+FWD).

Figure 25: Combined Results for AMB and TPJB compressors

The blue, stable zone for TPJB machine (Figure 25 right) forms a triangle: at positive K_{rad} (0°) the shaft handles lot of tangential force. Moving horizontally left, towards 180° (negative direct stiffness), the system carries less and less tangential force because the eigenfrequency ω_0 drops. The Flexible Ratio (FR) increases and, as described on the simplified approach (page 6), stabilizing associated seal WFR must be small.

Therefore, the combination of AMB machinery and negative stiffness generating seal conditions needs special care. As an example, heavy fouling can generate such negative stiffness. Kleynhans et al. (2016) discuss an increase in sub-synchronous vibration paired with a dropping piston leakage during the comprehensive wet gas testing period.

CONCLUSIONS

Stability Threshold References

Q_{r0} and Q_{t0} offer the opportunity to create reference charts for the future. Often risk estimation reverts to experience maps. At the beginning of this paper two maps classify the TPJB and AMB machines: Figure 1 (Critical Speed Ratio) and Figure 5 (Flexible Ratio). Both diagrams have the advantage that the needed data is (relatively) simple to compute, meaning that no, maybe inaccessible, machinery details are required. The CSR diagram doesn't need bearing and seal characteristics. The FR diagram does not need seal coefficients, but contains implicitly the bearing's data (see Figure 6). The generalized force approach calculations presented add to Level II analysis and require all seal data and extensive calculations.

The Q_{r0} and Q_{t0} assessment performed on the unloaded (instead of the loaded case presented) system offers an interesting alternative. The procedure is very close to a Level I screening, but the goal different. The radial and tangential stability thresholds shall not trigger or avoid deeper analysis yet serve as indicator for a general "seal impedance" load capacity attributed to the shaft-bearing system. Such a reference map (of unloaded Q_{r0} and Q_{t0}, which is of course Q_0) could generate high value when used to challenge the bearing selection and/or controller design.

A careful assessment of the compared machines is indispensable in the end.

Closure

Customers regularly require a third party analysis to confirm the high-pressure compressor rotordynamics. More and more the authors encounter additions to pure Level II analysis such as sensitivity checks, higher thresholds or additional load cases in the client specification. Those recalculations and additions prove end user awareness of purchasing demanding rotating equipment.
Therefore, an API Level I and II rotordynamic stability assessment extension to include radial force variation was applied to an oil bearing and an AMB equipped compressor. Based on the investigated machines shown here, the TPJB bearing machine stability degradation is most sensitive to tangential forces, while an AMB equipped machine is more sensitive to radial forces. Hence, the standard API 617 procedure to assess stability based on cross-coupled stiffness induced destabilizing tangential forces is appropriate for conventional oil bearing machines, but lacks full destabilizing force assessment for AMB machines. An AMB machine stability analysis that includes radial force variation with safety margin determination will provide additional confidence that a demanding machine application will have safe and stable field operation.

APPENDIX: NON-SYNCHRONOUS HARMONIC FORCES AT PISTON DURING DESTABILIZATION.

The homogeneous part of the differential equations does not fully cover the aeroacoustics. Accounting for the pressure field's harmonic excitation not reproducible in eigenvalue analysis, a constant force shall excite the rotor at piston location. The force applied corresponds to 1000 N for both the TPJB and the AMB machines.

The result key figures quantify the machine from a practical perspective: end user does not monitor operating compressors in log dec or eigenfrequencies but in shaft displacement vibrations. The comparison between the results and the measured vibration footprint evolution can indicate the nature of predominant seal coefficient the machine is facing.

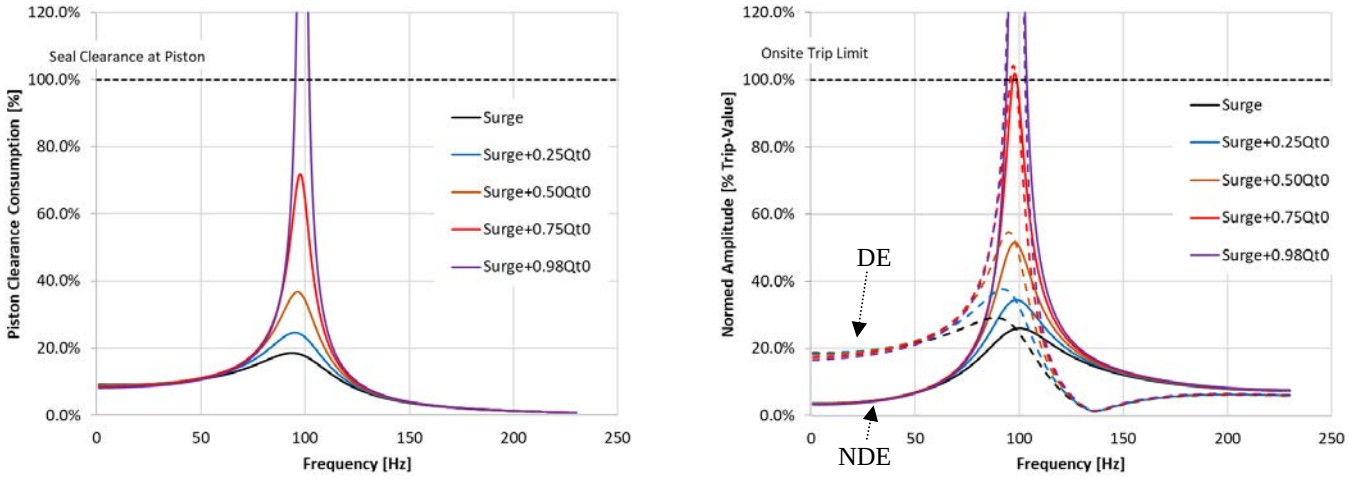

Figure 26: Force Response Analysis: TPJB machine (K_{tan} = 0.25 / 0.5 / 0.75 / 0.98xQ_{t0})

Figure 26 presents the non-synchronous excitation response for the TPJB machine excited at the basic load case "surge" and an additional Q_{t0} impedance fraction: the vibration at piston location compared to the minimum piston seal clearance (left) and the vibrations at the monitored sensor locations (right), plotted against the trip limit. The dotted lines represent the DE side of compressor, the solid lines the NDE. The sensor readings will trip the machine, when reaching 75% of the tangential stability threshold.

For a destabilisation along the negative stiffness axis (180° in Figure 20) Figure 27 shows the results in the same manner.

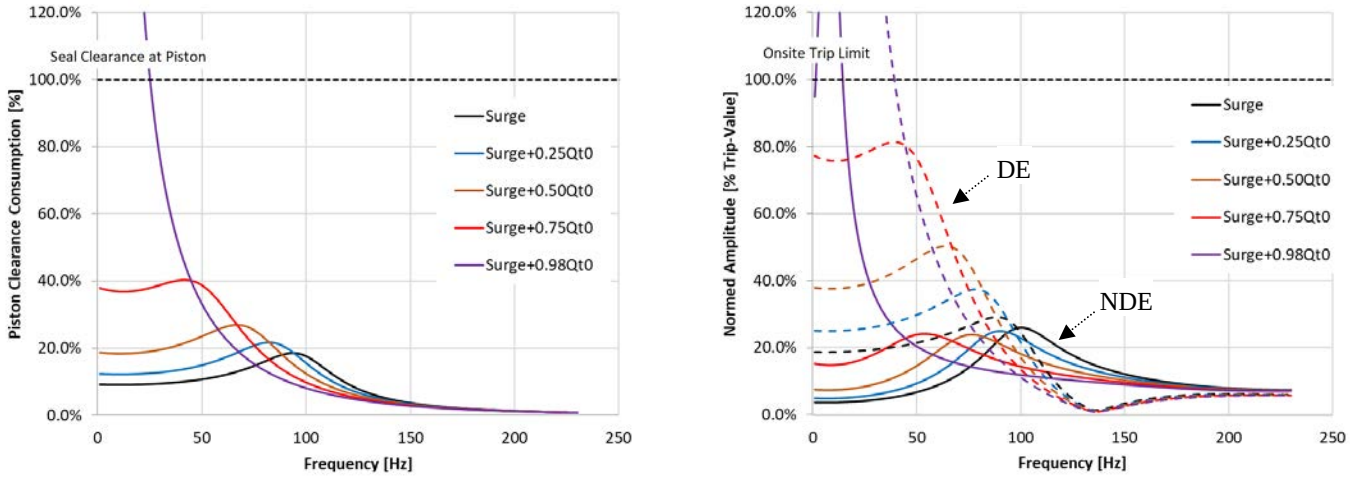

Figure 27: Force Response Analysis: TPJB machine (K_{rad} = 0.25 / 0.5 / 0.75 / 0.98x Q_{r0})

If negative stiffness is present in the system, then the sensitivity of the piston to a force excitation grows, even if the modal damping increases (recall Figure 16). The TPJB bearing rotor will show more and more noise below 100 Hz for the same aerodynamic excitation pattern. A vibration trip will shut down the unit at somewhat more than 75% of stability reserve consumption.

Figure 28 shows the results for the progressive cross-coupled stiffness AMB shaft destabilisation. The graph right side compares the two sensor readings next to the piston, compressor bearing (solid) and motor DE bearing sensors (dotted), to the AMB trip limit. The

trip limit, defined by a fraction of minimum catcher bearing clearance, is higher. Nevertheless, the vibration measurement protects the machine well before the shaft consumes the piston seal clearance (red line at 75% Q_{t0}) presented on the left side of Figure 28.

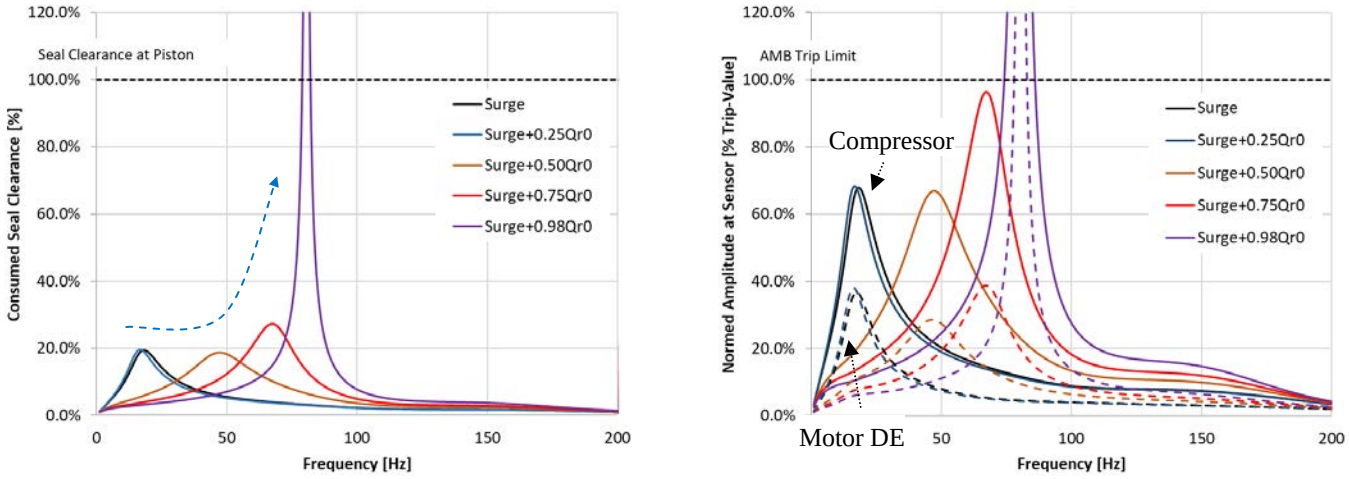

Figure 28: Force Response Analysis: AMB machine (K_{tan} = 0.25 / 0.5 / 0.75 / 0.98x Q_{t0})

Finally, the calculation presented in Figure 29 covers the direct negative stiffness destabilisation of forward mode. The compressor bearing reaches the trip limit first at a K_{rad}/Q_{r0} rate of 0.3 (compare to the blue line at 25%).

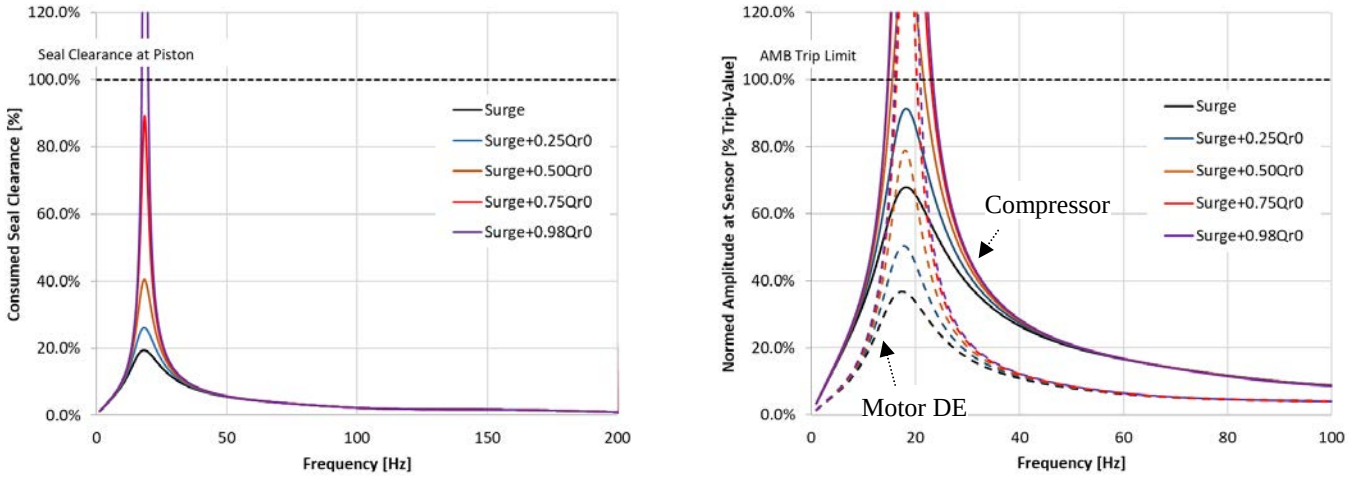

Figure 29: Force Response Analysis: AMB machine (K_{rad} = 0.25 / 0.5 / 0.75 / 0.98x Q_{r0})

Table 7 presents the key results overview concerning machine safety for the two instability scenarios “radial” and “tangential”.

Table 7: Piston clearance utilization at machine trip level vibration.

	AMB		TPJB	
Destabilisation direction	Trip triggered Stability Ratio [-]	Piston clearance utilization [%]	Trip triggered Stability Ratio [-]	Piston clearance utilization [%]
Tangential K_{tan} (+)	0.75	30	0.73	69
Radial K_{rad} (-)	0.29	30	0.75	50

The trip values settings protect both TPJB and AMB rotors.

NOMENCLATURE

General:

AMB	=	Active Magnetic Bearing (machine)	
API	=	American Petroleum Industry	
DGS	=	Dry Gas Seals	
FAT	=	Factory Acceptance Test	
OEM	=	Original Equipment Manufacturer	
BWD	=	Backward whirl direction	
FWD	=	Forward whirl direction	
CSR	=	Critical Speed Rigid Ratio	
N_{MC}	=	Maximum continuous operating speed	[rpm]
TPJB	=	Oil-film Lubricated bearing (machine)	

Bearings and seal coefficients:

Kxx, Kyy	=	Direct Stiffness Coefficient	[N/m]
Kxy, Kyx	=	Cross-Coupled Stiffness Coefficient	[N/m]
Dxx, Dxx	=	Direct Damping Coefficient	[Ns/m]
Dxy, Dyx	=	Cross-Coupled Damping Coefficient	[Ns/m]
A	=	Amplitude	[µm]
ω	=	Whirl frequency	[rad/s]
F_{rad}	=	Radial Force	[N]
F_{tan}	=	Tangential Force	[N]
G	=	Gain (resultant force)	[N]
φ	=	Impedance phase	[°]
ε	=	Eccentricity	[m]
PID	=	proportional–integral–derivative controller	

Level I Analysis:

N_{modeA}	=	Modal Frequency at Q_A	[cpm]
δ	=	Logarithmic decrement	[-]
Q_A	=	Anticipated Cross-Coupled Stiffness	[N/µm]
δ_A	=	Logarithmic decrement at Q_A	[-]
Q_0	=	Stability Threshold	[N/µm]

Level II Analysis:

N_{mode}	=	Modal Frequency (loaded)	[cpm]
δ_f	=	Final Logarithmic decrement	[-]

Simplified Approach:

Ω	=	Shaft rotational speed	[1/s]
WFR	=	Whirl Frequency Ratio	[-]
FR	=	Flexible Ratio (ratio Ω/ ω)	[-]

Robustness to Cross-Coupled Stiffness:

Q_{t0}	=	Stab. Thr. Cross-Coupled Stiffness	[N/µm]
ω_{t0}	=	Whirl frequency at Q_{t0}	[rad/s]

Robustness to Direct Stiffness:

Q_{r0}	=	Stability Threshold Direct Stiffness	[N/µm]
ω_{r0}	=	Whirl frequency at Q_{r0}	[rad/s]

Robustness to Generalized Force:

K	=	Gain, Added Impedance Magnitude	[N/µm]
φ	=	Added Impedance phase	[°]
K_{rad}	=	Direct Stiffness (φ=0°)	[N/µm]
K_{tan}	=	Cross-Coupled Stiffness (φ=90°)	[N/µm]

REFERENCES

API 617, 2014, “Axial and Centrifugal Compressors and Expender-compressors”, Eighth Edition, American Petroleum Institute, Washington, D.C.

API 684, 2005, “API Standard Paragraphs Rotordynamic Tutorial: Lateral Critical Speeds, Unbalance Response, Stability, Train Torsionals and Rotor Balancing”, Second Edition, American Petroleum Institute, Washington, D.C.

Baumann, U., 2011, “Stability Considerations – A Simplified Approach”, Proceedings of the First Middle East Turbomachinery Symposium, Doha, Qatar

Camatti, M., Vannini, G., Fulton, J. W. and Hopenwasser, F., 2003, “Instability of a High Pressure Compressor equipped with Honeycomb Seals”, Proceedings of the thirty-second Turbomachinery Symposium, Turbomachinery Laboratory, Texas A&M University, College Station, Texas, USA, doi: 10.21423/R1636F

Cloud, C.H., Kocur, Jr. J.A. and Pettinato, B. C., 2018, “Predicting, Understanding and Avoiding the Ekofisk Rotor Instability Forty Years Later”, Proceedings of the Forty-Seventh Turbomachinery Symposium, Texas A&M University, College Station, Texas, USA, doi: 1969.1/174995

Dettwyler, M., Büche, D. and Baumann, U., 2016, “Subsea Compression – Current Technology and its Use to Maximize Late Life Production”, Proceedings of the Forty-Fifth Turbomachinery Symposium, Texas A&M University, College Station, Texas, USA, doi: 10.21423/R1Z593

Eldridge, T. and Soulas, T., 2005, “Mechanism and Impact of Damper Seal Clearance Divergence on the Rotordynamics of Centrifugal Compressors”, Proceedings of GT2005 Symposium, ASME Turbo Expo 2005, Reno-Tahoe, Nevada, USA

Evans, B., F. and Fulton, J. W., 2010, “Wachel’s Equation – Origin and Current Evaluation of API 617 Rotor Stability Criteria”, Proceedings of the Thirty-Ninth Turbomachinery Symposium, Texas A&M University, College Station, Texas, USA, doi: 10.21423/R15932

Fulton, J.W., 1984, “The Decision to Full Load Test a High Pressure Centrifugal Compressor in its Module Prior to Tow-out”, IMechE, Second European Congress, Fluid Machinery for the Oil, The Hague, The Netherlands

ISO, 2006, “ISO 14939-3: Mechanical vibration – Vibration of rotating machinery equipped with active magnetic bearings - Part 3: Evaluation of stability margin.”

Kleynhans, G., Pfrehm, G., Berger and H., Baudelocque, L., 2005, “Hermetically Sealed Oil-Free Turbocompressor Technology”, Proceedings of the Thirty-Fourth Turbomachinery Symposium, Texas A&M University, College Station, Texas, USA, doi: 10.21423/R1X36Z

Kleynhans, G., Brenne, L., Kibsgaard, S. and Dentu, P., 2016, “Development and Qualification of a Subsea Compressor”, Proceedings Offshore Technology Conference, Houston, Texas, USA, doi:10.4043/27160-MS

Kocur, J.A., Nicholas, J. C. and Lee, C. C., 2007, “Surveying Tilting Pad Journal Bearing and Gas Labyrinth Seal Coefficients and Their Effect on Rotor Stability”, Proceedings of the Thirty-Sixth Turbomachinery Symposium, Texas A&M University, College Station, Texas, USA, doi: 10.21423/R16S83

Kocur, J.A. and Cloud, C. H., 2013, “Shop Rotordynamic Testing – Options, Objectives, Benefits and Practices”, Proceedings of the Forty-Second Turbomachinery Symposium, Texas A&M University, College Station, Texas, USA, doi: 10.21423/R1GD2H

Moore, J., Camatti, M., Smalley, A., Vannini, G. and Vermin, L., 2006, “Investigation of a Rotordynamic Instability in a High Pressure Centrifugal Compressor Due to Damper Seal Clearance Divergence”, 7th IFToMM, Vienna, Austria.

Somaini, R., Baumann, U. and Bidaut, Y., 2012, “Comparison of Different Variable Speed Compression Train Configurations With Respect to Rotordynamic Stability and Torsional Integrity”, Proceedings of the Forty-First Turbomachinery Symposium, Texas A&M University, College Station, Texas, USA, doi: 10.21423/R1MS8T

Smithanik, J. and Paul, Y., 2015, “Applying API 617, 8th Edition to Expander-Compressors with Active Magnetic Bearings”, Proceedings of the Forty-Forth Turbomachinery Symposium, Texas A&M University, College Station, Texas, USA, doi: 10.21423/R13D0B

Sood,V. K., 1979, "Design and Full Load Testing of a High Pressure Centrifugal Natural Gas Injection Compressor", Proceedings of the Eighth Turbomachinery Symposium, Texas A&M University, College Station, Texas, USA, doi: 10.21423/R1X95N

Swanson, E., Masala, A. and Hawkins, L., 2014, "New Active Magnetic Bearing Requirements for Compressors in API Eight Edition", Proceedings of the Forty-Third Turbomachinery Symposium, Texas A&M University, College Station, Texas, USA, doi: 10.21423/R1WD27

Wachel, J. C. and von Nimitz, W.W., 1981, "Ensuring the Reliability of Offshore Gas Compression Systems", Journal of Petroleum Technology, AIME